



HAL
open science

Identification of potent indolizine derivatives against Mycobacterial tuberculosis: In vitro anti-TB properties, in silico target validation, molecular docking and dynamics studies

Katharigatta Venugopala, Sandeep Chandrashekarappa, Pran Kishore Deb, Nizar Al-Shar'I, Melendhran Pillay, Priya Tiwari, Deepak Chopra, Pobitra Borah, Rasoul Tamhaev, Lionel Mourey, et al.

► To cite this version:

Katharigatta Venugopala, Sandeep Chandrashekarappa, Pran Kishore Deb, Nizar Al-Shar'I, Melendhran Pillay, et al.. Identification of potent indolizine derivatives against Mycobacterial tuberculosis: In vitro anti-TB properties, in silico target validation, molecular docking and dynamics studies. *International Journal of Biological Macromolecules*, 2024, 274 (Part 2), pp.133285. 10.1016/j.ijbiomac.2024.133285 . hal-04739866

HAL Id: hal-04739866

<https://hal.science/hal-04739866v1>

Submitted on 16 Oct 2024

HAL is a multi-disciplinary open access archive for the deposit and dissemination of scientific research documents, whether they are published or not. The documents may come from teaching and research institutions in France or abroad, or from public or private research centers.

L'archive ouverte pluridisciplinaire **HAL**, est destinée au dépôt et à la diffusion de documents scientifiques de niveau recherche, publiés ou non, émanant des établissements d'enseignement et de recherche français ou étrangers, des laboratoires publics ou privés.

Identification of potent indolizine derivatives against *Mycobacterium tuberculosis*: *In vitro* anti-TB properties, *in silico* target validation, molecular docking and dynamics studies

Katharigatta N. Venugopala^{1,2,*}, Sandeep Chandrashekarappa^{3*}, Pran Kishore Deb^{4,*}, Nizar A. Al-Shar'i^{5,6}, Melendhran Pillay⁷, Priya Tiwari³, Deepak Chopra⁸, Pobitra Borah⁹, Rasoul Tamhaev^{10,11}, Lionel Mourey¹¹, Christian Lherbet¹⁰, Bandar E. Aldhubiab¹, Christophe Tratrat¹, Mahesh Attimarad¹, Anroop B. Nair¹, Nagaraja Sreeharsha^{1,12}, Raghu Prasad Mailavaram¹³, Rashmi Venugopala¹, Viresh Mohanlal², Mohamed A. Morsy^{1,15},

¹ Department of Pharmaceutical Sciences, College of Clinical Pharmacy, King Faisal University, Al-Ahsa 31982, Saudi Arabia; momorsy@kfu.edu.sa (M.A.M.); baldhubiab@kfu.edu.sa (B.E.A.); ctratrat@kfu.edu.sa (C.T.); mattimarad@kfu.edu.sa (M.A.); anair@kfu.edu.sa (A.B.N.); sharsha@kfu.edu.sa (N.S.);

² Department of Biotechnology and Food Science, Faculty of Applied Sciences, Durban University of Technology, Durban, 4000, South Africa; vireshm@dut.ac.za (V.M.)

³ Department of Medicinal Chemistry, National Institute of Pharmaceutical Education and Research (NIPER-R) Raebareli, Lucknow (UP) 226002, India; c.sandeep@niperraebareli.edu.in (S.C.)

⁴ Department of Pharmaceutical Sciences and Technology, Birla Institute of Technology (BIT), Mesra, Ranchi 835215, Jharkhand, India; prankishore1@gmail.com; prankishoredeb@bitmesra.ac.in (P.K.D.)

⁵ Department of Medicinal Chemistry and Pharmacognosy, Faculty of Pharmacy, Jordan University of Science and Technology, P.O. Box 3030, Irbid 22110, Jordan; nashari@just.edu.jo (N.A.A.)

⁶ Department of Pharmaceutical Sciences, College of Pharmacy, Qatar University, P.O. Box: 2713, Doha, Qatar

⁷ Department of Microbiology, National Health Laboratory Services, KZN Academic Complex, Inkosi Albert Luthuli Central Hospital, Durban 4001, South Africa; melendhra.pillay@nhls.ac.za (M.P.)

⁸ Department of Chemistry, Indian Institute of Science Education and Research Bhopal, Bhopal By-pass Road, Bhauli, Bhopal 462066, Madhya Pradesh, India; dchopra@iiserb.ac.in (D.C.)

⁹ Department of Biological Sciences and Bioengineering, Indian Institute of Technology (IIT), Kanpur 208016, Uttar Pradesh, India. E-mails: pborah22@iitk.ac.in (P.B.)

¹⁰ Synthèse et Physico-Chimie de Molécules d'Intérêt Biologique (LSPCMIB), UMR 5068, CNRS, Université Toulouse III – Paul Sabatier (UT3), Toulouse, France; rasoul.tamhaev@gmail.com (R.T.); christian.lherbet@univ-tlse3.fr (C.L.)

¹¹ Institut de Pharmacologie et de Biologie Structurale (IPBS), Université de Toulouse, CNRS, Université Toulouse III – Paul Sabatier (UPS), Toulouse, France; lionel.mourey@ipbs.fr (L.M.)

¹² Department of Pharmaceutics, Vidya Siri College of Pharmacy, Off Sarjapura Road, Bangalore 560035, India;

¹³ Department of Pharmaceutical Chemistry, Shri Vile Parle Kelavani Mandal's Institute of Pharmacy, Samtanagar, Dhule 424 001, Maharashtra, India; raghuprasad.mailavaram@svkm.ac.in (R.P.M.)

¹⁴ Department of Public Health Medicine, Howard College Campus, University of KwaZulu-Natal, Durban 4001, South Africa; rashmivenugopala@gmail.com (R.V.)

¹⁵ Department of Pharmacology, Faculty of Medicine, Minia University, El-Minia 61511, Egypt

*Address correspondence to:

1. **Dr. Katharigatta N. Venugopala**, Professor, Department of Pharmaceutical Sciences, College of Clinical Pharmacy, King Faisal University, Al-Ahsa 31982, Saudi Arabia: Tel: +966-1358-98842 E-mail: kvenugopala@kfu.edu.sa; ORCID: <https://orcid.org/0000-0003-0680-1549>
2. **Dr. Sandeep Chandrashekarappa**, Assistant Professor, Department of Medicinal Chemistry, National Institute of Pharmaceutical Education and Research (NIPER-R) Raebareli, Lucknow (UP)-226002, India; E-mail: c.sandeep@niperraebareli.edu.in; ORCID: <https://orcid.org/0000-0003-2475-7270>
3. **Dr. Pran Kishore Deb**, Associate Professor, Department of Pharmaceutical Sciences and Technology, Birla Institute of Technology (BIT), Mesra, Ranchi 835215, Jharkhand, India; prankishore1@gmail.com; prankishoredeb@bitmesra.ac.in (P.K.D.) ORCID: <http://orcid.org/0000-0002-8650-2874>

Abstract

In the current study, two sets of compounds: (*E*)-1-(2-(4-substitutedphenyl)-2-oxoethyl)-4-((hydroxyimino)methyl)pyridinium derivatives (**3a-3e**); and (*E*)-3-(substitutedbenzoyl)-7-((hydroxyimino)methyl)-2-substitutedindolizine-1-carboxylate derivatives (**5a-5j**), were synthesized and biologically evaluated against two strains of *Mycobacterium tuberculosis*; H37Rv and MDR. Further, they were also tested *in vitro* against the mycobacterial InhA enzyme. The *in vitro* results showed excellent inhibitory activities against both MTB strains, and compounds **5a-5j** were found to be more potent and their MIC values ranged from 5-16 µg/mL and 16-64 µg/mL against the H37Rv and MDR-TB strains, respectively. Compound **5h** with phenyl and 4-fluorobenzoyl groups attached to the 2- and 3-position of the indolizine core was found to be the most active against both strains with MIC values of 5 µg/mL and 16 µg/mL, respectively. On the other hand, the two sets of compounds showed weak to moderate inhibition of InhA enzyme activity that ranged from 5-17% and 10-52%, respectively, with compound **5f** containing 4-fluoro benzoyl group attached to the 3-position of the indolizine core being the most active (52% inhibition of InhA). Unfortunately, there was no clear correlation between the InhA inhibitory activity and MIC values of the tested compounds indicating the probability that they might have different modes of action other than InhA inhibition.

Therefore, a computational investigation was conducted by employing molecular docking in order to identify their putative drug target(s), consequently, understand their mechanism of action. A panel of 20 essential mycobacterial enzymes was investigated, of which β-ketoacyl acyl carrier protein synthase I (KasA) and pyridoxal-5'-phosphate (PLP)-dependent aminotransferase (BioA) enzymes were revealed as the putative targets for compounds **3a-3e** and **5a-5j**, respectively. Moreover, *in silico* ADMET predictions showed adequate properties for these compounds, making them promising leads worthy of further optimization.

Keywords: 2-substitutedindolizine; *Mycobacterium tuberculosis*; multidrug-resistant *Mycobacterium tuberculosis*; Molecular docking; molecular dynamics simulations; MTB target validation.

1. Introduction

Tuberculosis (TB) has been known to affect human beings for millennia with a high mortality rate (1), and the control of TB remains one of the largest endeavors of public health authorities ever since the identification of the causative organism *Mycobacterium tuberculosis* (MTB) by Robert Koch in the year 1882 (2). Although predominantly a pulmonary pathogen, MTB can evade throughout the body and can manifest a dynamic spectrum, from asymptomatic infection (latent TB infection or LTBI) to a transmissible life-threatening (active TB) disease (3-5). The global TB targets of Sustainable Development Goals (SDGs) and End TB strategy have anticipated milestones like an 80% decline in TB incidence rate and a 90% reduction in annual TB deaths by 2030 (6). Nonetheless, the world as a whole is still out of track to achieve these goals, and TB yet remains a major global public health burden, being responsible for 1.4 million deaths and 10 million infections worldwide in 2019. Additionally, about 2 billion people are reported to be infected with TB, of which only 5-10% of people possess the risk of TB eruption as a full-blown disease during their lifetime (7); however, the risk increases dramatically in case of perturbation of the immune responses (e.g., in HIV infections), and among people with risk factors like undernutrition, smoking, diabetes or alcoholism (8).

The treatment strategy for drug-susceptible TB (DS-TB) consists of a six-month course of 4 first-line anti-TB drugs, *viz.* rifampicin, isoniazid, pyrazinamide, and ethambutol (9, 10). Nevertheless, the steady advent of drug resistance to the first-line drugs over time culminated in the identification of mono-resistance TB or multi-drug resistant TB (MDR-TB), at least to isoniazid and rifampicin. Unfortunately, 465,000 new rifampicin-resistant TB (RR-TB) cases were reported in 2019, of which 78% of cases were MDR-TB and were responsible for 182,000 deaths (6). In addition to the longer treatment duration, expensive therapy, and higher toxicity associated with RR-TB/MDR-TB regimen (11, 12), increasing prevalence of extensively drug-resistance TB or XDR-TB (i.e., MTB resistance to isoniazid, rifampicin, and additional resistance to a fluoroquinolone and a second-line injectable) and totally drug-resistant TB (TDR-TB) is miserable. Despite the higher attrition rate in the anti-TB drug discovery, currently, clinical trials of 23 potential anti-TB drugs are underway; of them, 13 are novel compounds that include bedaquiline, delamanid, and pretomanid, which are already approved by the regulatory authorities (13-15). Though a plethora of MTB inhibitory molecules is under development or available for clinical use, more concerning is the rapid emergence of the resistant strains against the newer drugs, as exemplified by the appearance of the bedaquiline and delamanid resistant MTB clinical isolates within two years from approval (16). Apart from this, the ineffectiveness of these newer drugs (like bedaquiline and delamanid) against TDR-TB is also disappointing (17). Together all these issues clearly indicate the compelling demand for newer effective molecules capable of overcoming MTB resistance to halt the progress of drug resistance.

To this end, our research efforts focused towards the development of novel compounds with different chemotypes as potent anti-TB agents. During the past few years we had designed, synthesized, and reported several compounds with different chemotypes as potential anti-TB agents, comprising natural products, cyclic depsipeptides, and compounds belonging to various heterocyclic scaffolds such as aminoquinazolines, benzothiazoles, pyrrolo[1,2-*a*]quinolines, dihydropyrimidines, tetrahydropyrimidinones, and tetrahydropyrimidinethiones, 1-(5-isoquinolinesulfonyl)piperazines, triazoles, triazolyl 1,2,3,4-tetrahydropyrimidines, various substituted indolizines, and various substituted 1,2,4-oxadiazoles (18-35).

Recently we have synthesized and patented a novel series of (*E*)-1-(2-(4-substitutedphenyl)-2-oxoethyl)-4-((hydroxyimino)methyl)pyridinium derivatives, and (*E*)-3-(substitutedbenzoyl)-7-((hydroxyimino)methyl)-2-substitutedindolizine-1-carboxylate derivatives (36). In the current study, the anti-tubercular activity of these compounds was biologically evaluated against H37Rv and MDR strains of MTB. Also, they were tested (*in vitro*) against the mycobacterial InhA enzyme. Moreover, computational studies were also implemented aiming to identify their potential mycobacterial target to get an insight into their probable mechanism of action.

2. Experimental

2.1. Materials and Methods

The chemicals reported here were obtained from Sigma-Aldrich Co. (St. Louis, MO, USA), while the solvents were obtained from Millipore Sigma (Burlington, MA, USA). Thin-layer chromatography (TLC) using silica gel (Sigma-Aldrich Co.) on aluminum foil was employed to observe the chemical reactions; n-hexane and ethyl acetate (4:6) were used as the solvent. The reactions were visualized under an ultraviolet (UV)-light/iodine chamber. B-545 was used to measure the melting points (Büchi, Labortechnik, Flawil, Switzerland). The Fourier Transform-Infrared (FT-IR) spectra were recorded on a Shimadzu FT-IR spectrophotometer. Furthermore, ¹H and ¹³C-NMR spectra were recorded on Bruker AVANCE III 400 MHz instruments using DMSO-*d*₆ as a solvent. Chemical shifts (δ) were recorded in parts per million (ppm) downfield from tetramethylsilane; then, the coupling constants (J) were recorded in Hertz. The splitting pattern was documented as follows: s, singlet; d, doublet; q, quartet; and m, multiplet. Liquid chromatography-mass spectrometry (LC-MS; Agilent 1100 series) was used to measure the mass spectra in conjunction with MSD, and 0.1% aqueous trifluoroacetic acid in an acetonitrile system on the C18-BDS column. Then, the elemental analysis was carried out using the analyzer FLASH EA 1112 CHN (Thermo Finnigan LLC, New York, NY, USA). A single-crystal X-ray diffraction study was performed using a Bruker KAPPA APEX II DUO

diffractometer equipped with a CCD detector,; monochromated Mo K α radiation ($\lambda = 0.71073 \text{ \AA}$) was used. Data collection was carried out at 173(2) K using an Oxford Cryostream cooling system featuring the Bruker Apex II software.

2.2. Chemistry

The two sets of compounds (*E*)-1-(2-(4-substituedphenyl)-2-oxoethyl)-4-((hydroxyimino)methyl)pyridinium derivatives (**3a-3e**), and (*E*)-3-(substituedbenzoyl)-7-((hydroxyimino)methyl)-2-substituedindolizine-1-carboxylate derivatives (**5a-5j**) were synthesized by following scheme 1.

2.3. General Synthetic Procedure for the Preparation of (*E*)-1-(2-(substituedphenyl)-2-oxoethyl)-4-((hydroxyimino)methyl)pyridin-1-ium bromides (**3a-e**)

To a stirred solution of 4-pyridine aldoxime (0.0081 mol) in dry acetone (10 mL), was added substituted phenacyl bromide (0.0081 mol) and stirred at room temperature for 30 min. Solid formed was separated, filtered, and dried under vacuum to afford the (*E*)-1-(2-(substituedphenyl)-2-oxoethyl)-4-((hydroxyimino)methyl)pyridin-1-ium bromides at 95-98% yield.

2.3.1. (*E*)-4-((Hydroxyimino)methyl)-1-(2-oxo-2-phenylethyl)pyridin-1-ium bromide (**3a**)

Appearance - white amorphous compound; Yield - 95%; m.p. - 215-216 °C; FT-IR in cm^{-1} : 3022, 1693, 1639, 1581, 1517, 1400; $^1\text{H-NMR}$ (400 MHz, $\text{DMSO-}d_6$); 12.94 (1H, s), 8.94-8.93 (2H, d, $J = 6.2 \text{ Hz}$), 8.48 (1H, s), 8.36-8.34 (2H, d, $J = 7.2 \text{ Hz}$), 8.08-8.06 (2H, d, $J = 7.2 \text{ Hz}$), 7.82-7.81 (1H, m), 7.79-7.66 (2H, m), 6.45 (2H, s); $^{13}\text{C-NMR}$ (100 MHz, $\text{DMSO-}d_6$); 190.72, 149.08, 146.44, 145.24, 134.73, 133.50, 129.14, 128.23, 123.79, 65.78; HRMS (ESI-TOF) (m/z): $[\text{M}+\text{H}]^+$ calculated for $\text{C}_{14}\text{H}_{13}\text{BrN}_2\text{O}_2$, 241.0972; found, 241.1241.

2.3.2. (*E*)-1-(2-(4-Bromophenyl)-2-oxoethyl)-4-((hydroxyimino)methyl)pyridin-1-ium bromide (**3b**)

Appearance - white amorphous compound; Yield – 97%; m.p. - 247-248 °C; FT-IR in cm^{-1} : 3020, 1693, 1639, 1579, 1400, 532; $^1\text{H-NMR}$ (400 MHz, $\text{DMSO-}d_6$); 12.94 (1H, s), 8.94-8.93 (2H, d, $J = 6.2 \text{ Hz}$), 8.48 (1H, s), 8.36-8.35 (2H, d, $J = 7.2 \text{ Hz}$), 8.01-7.99 (2H, d, $J = 7.2 \text{ Hz}$), 7.92-7.90 (2H, d, $J = 7.2 \text{ Hz}$), 6.45 (2H, s); $^{13}\text{C-NMR}$ (100 MHz, $\text{DMSO-}d_6$); 190.14, 149.14, 146.42, 145.23, 132.60, 132.24, 130.16, 128.81, 123.80, 65.68; HRMS (ESI-TOF) (m/z): $[\text{M}+\text{H}]^+$ calculated for $\text{C}_{14}\text{H}_{12}\text{Br}_2\text{N}_2\text{O}_2$, 319.0077; found, 319.0328.

2.3.3. (*E*)-1-(2-(4-Fluorophenyl)-2-oxoethyl)-4-((hydroxyimino)methyl)pyridin-1-ium bromide (3c)

Appearance - white amorphous compound; Yield – 96%; m.p. - 223-224 °C; FT-IR in cm^{-1} : 3029, 1697, 1639, 1514, 1454, 1230; $^1\text{H-NMR}$ (400 MHz, $\text{DMSO-}d_6$); 12.93 (1H, s), 8.98-8.96 (2H, d, $J = 6.2$ Hz), 8.49 (1H, s), 8.37-8.35 (2H, d, $J = 7.2$ Hz), 8.19-8.15 (2H, m), 7.54-7.50 (2H, m), 6.49 (2H, s); $^{13}\text{C-NMR}$ (100 MHz, $\text{DMSO-}d_6$); 189.47, 167.00, 164.48, 149.11, 146.42, 145.21, 131.47, 131.37, 130.36, 130.34, 123.79, 116.41, 116.19, 65.68; HRMS (ESI-TOF) (m/z): $[\text{M}+\text{H}]^+$ calculated for $\text{C}_{14}\text{H}_{12}\text{BrFN}_2\text{O}_2$, 338.0066; found, 259.1282.

2.3.4. (*E*)-1-(2-(4-Cyanophenyl)-2-oxoethyl)-4-((hydroxyimino)methyl)pyridin-1-ium bromide (3d)

Appearance - white amorphous compound; Yield – 98%; m.p. - 236-237 °C; FT-IR in cm^{-1} : 3028, 2223, 1699, 1641, 1596; $^1\text{H-NMR}$ (400 MHz, $\text{DMSO-}d_6$); 12.95 (1H, s), 8.95-8.93 (2H, d, $J = 7.2$ Hz), 8.49 (1H, s), 8.38-8.36 (2H, d, $J = 7.2$ Hz), 8.23-8.16 (4H, m), 6.49 (2H, s); $^{13}\text{C-NMR}$ (100 MHz, $\text{DMSO-}d_6$); 190.33, 149.23, 146.42, 145.24, 136.80, 133.10, 128.84, 123.85, 117.93, 116.29, 65.95; HRMS (ESI-TOF) (m/z): $[\text{M}+\text{H}]^+$ calculated for $\text{C}_{15}\text{H}_{12}\text{BrN}_3\text{O}_2$, 345.0133; found, 266.1128.

2.3.5. (*E*)-4-((Hydroxyimino)methyl)-1-(2-(2-nitrophenyl)-2-oxoethyl)pyridin-1-ium bromide (3e)

Appearance - white amorphous compound; Yield – 98%; m.p. - 241-242 °C; FT-IR in cm^{-1} : 3029, 1695, 1639, 1508, 1396; $^1\text{H-NMR}$ (400 MHz, $\text{DMSO-}d_6$); 12.97 (1H, s), 8.98-8.96 (2H, d, $J = 6.2$ Hz), 8.50 (1H, s), 8.43-8.41 (2H, d, $J = 7.2$ Hz), 8.30-8.28 (1H, d, $J = 7.2$ Hz), 8.10-8.04 (2H, d, m), 7.96-7.92 (1H, m), 6.39 (2H, s); $^{13}\text{C-NMR}$ (100 MHz, $\text{DMSO-}d_6$); 192.79, 149.50, 146.14, 145.92, 145.23, 134.67, 133.21, 131.24, 128.88, 124.65, 124.65, 124.11, 66.82; HRMS (ESI-TOF) (m/z): $[\text{M}+\text{H}]^+$ calculated for $\text{C}_{14}\text{H}_{12}\text{BrN}_3\text{O}_4$, 365.0011; found, 286.0866.

2.4. Synthetic Procedure for the Preparation of Ethyl (*E*)-3-(substitutedbenzoyl)-7-((hydroxyimino)methyl)-2-methylindolizine-1-carboxylates (5a-j)

To a stirred solution of (*E*)-1-(2-(substitutedphenyl)-2-oxoethyl)-4-((hydroxyimino)methyl)pyridin-1-ium bromides (**3a-e**) (0.0031 mol), in dry DMF, was added substituted ethyl propiolate (0.0031 mol), K_2CO_3 (0.0068 mol), and stirred at room temperature for 30 min. Completion of the reaction was monitored by TLC. After completion, the reaction medium was evaporated under reduced pressure and diluted with ethyl acetate. The ethyl acetate layer was washed with brine, water and dried with anhydrous sodium sulfate. The ethyl acetate was removed under reduced pressure, and the crude compound was purified with a column using 60-120 mesh silica gel with ethyl acetate and hexane as

an eluent to afford 49-62% yield of ethyl (*E*)-3-(substitutedbenzoyl)-7-((hydroxyimino)methyl)-2-methylindolizine-1-carboxylates (**5a-j**).

2.4.1. Ethyl (*E*)-3-benzoyl-7-((hydroxyimino)methyl)indolizine-1-carboxylate (**5a**)

Appearance - brown compound; Yield – 60%; m.p. - 173-174 °C; FT-IR in cm^{-1} : 3380, 1697, 1593, 1571, 1525, 1469; $^1\text{H-NMR}$ (400 MHz, CDCl_3); δ = 9.77-9.76 (1H, d, J = 6.8 Hz), 8.28 (1H, s), 8.12 (1H, s), 7.75-7.71 (3H, m), 7.51-7.38 (4H, m), 4.33-4.29 (2H, q, J = 7.2Hz), 1.33-1.30 (3H, t, J = 7.2Hz); $^{13}\text{C-NMR}$ (100 MHz, CDCl_3); δ = 185.78, 163.97, 162.94, 148.09, 139.55, 139.34, 132.32, 131.93, 131.76, 130.16, 129.32, 129.04, 125.60, 123.36, 119.27, 114.82, 111.54, 107.68, 60.39, 14.52; HRMS (ESI-TOF) (m/z): $[\text{M}+\text{H}]^+$ calculated for $\text{C}_{19}\text{H}_{16}\text{N}_2\text{O}_4$, 337.1110; found, 337.1555.

2.4.2. Ethyl (*E*)-3-(4-fluorobenzoyl)-7-((hydroxyimino)methyl)indolizine-1-carboxylate (**5b**)

Appearance - brown compound; Yield – 53%; m.p. - 187-188 °C; FT-IR in cm^{-1} : 3269, 1681, 1600, 1573, 1529, 1467, 1222; $^1\text{H-NMR}$ (400 MHz, CDCl_3); δ = 9.75-9.76 (1H, m), 8.70 (1H, s), 8.29 (1H, s), 8.12 (1H, s), 7.79-7.68 (2H, m), 7.44-7.39 (1H, m), 7.15-6.99 (2H, m); $^{13}\text{C-NMR}$ (100 MHz, CDCl_3); δ = 184.22, 165.29, 164.25, 163.90, 149.34, 148.00, 147.48, 139.38, 135.73, 132.71, 131.65, 131.39, 129.28, 128.76, 125.65, 124.01, 123.11, 121.32, 119.24, 115.73, 114.88, 111.59, 107.72, 60.92, 14.51; MS (ESI Positive): m/z = (M+H) = 355.2; HRMS (ESI-TOF) (m/z): $[\text{M}+\text{H}]^+$ calculated for $\text{C}_{19}\text{H}_{15}\text{FN}_2\text{O}_4$, 355.1066; found, 355.1157.

2.4.3. Ethyl (*E*)-3-(4-cyanobenzoyl)-7-((hydroxyimino)methyl)indolizine-1-carboxylate (**5c**)

Appearance - yellow compound; Yield – 55%; m.p. - 175-176 °C; FT-IR in cm^{-1} : 3328, 2362, 1697, 1602, 1525, 1454, 1423; $^1\text{H-NMR}$ (400 MHz, CDCl_3); δ = 9.97-9.95 (1H, m), 8.83 (1H, s), 8.34 (1H, s), 8.14 (1H, s), 7.68-7.44 (5H, m), 7.19-7.14 (1H, m), 4.35-4.30 (2H, q, J = 7.2Hz), 1.36-1.33 (3H, t, J = 7.2Hz); $^{13}\text{C-NMR}$ (100 MHz, CDCl_3); δ = 189.75, 163.57, 148.21, 143.33, 134.01, 132.51, 132.46, 132.31, 130.60, 129.45, 129.05, 128.89, 125.33, 119.47, 117.96, 115.43, 112.03, 111.12, 108.42, 60.87, 14.51; HRMS (ESI-TOF) (m/z): $[\text{M}+\text{H}]^+$ calculated for $\text{C}_{20}\text{H}_{15}\text{N}_3\text{O}_4$, 362.1063; found, 362.1215.

2.4.4. Ethyl (*E*)-7-((hydroxyimino)methyl)-3-(2-nitrobenzoyl)indolizine-1-carboxylate (**5d**)

Appearance - brown compound; Yield – 56%; m.p. - 144-145 °C; FT-IR in cm^{-1} : 3450, 2923, 1691, 1620, 1521, 1467; $^1\text{H-NMR}$ (400 MHz, CDCl_3); δ = 9.94-9.92 (1H, m), 8.58-8.57 (1H, m), 8.28 (1H, s), 8.16 (1H, s), 8.14-8.13 (1H, m), 8.04 (1H, s), 7.73-69 (1H, m), 7.64-7.45 (2H, m), 4.30-4.25 (2H, q, J = 7.2Hz), 1.31-1.27 (3H, t, J = 7.2Hz); $^{13}\text{C-NMR}$ (100 MHz, CDCl_3); δ = 183.45, 162.95, 149.43, 147.82, 146.76, 140.90, 139.75, 135.72, 134.16, 133.88, 132.80, 131.09, 130.66, 129.32, 129.03, 128.09,

127.92, 125.73, 125.00, 124.86, 122.90, 121.30, 119.20, 112.17, 108.21, 61.00, 29.16, 14.48; HRMS (ESI-TOF) (m/z): [M+H]⁺ calculated for C₁₉H₁₅N₃O₆, 382.0961; found, 382.1124.

2.4.5. Ethyl (E)-3-(4-bromobenzoyl)-7-((hydroxyimino)methyl)-2-methylindolizine-1-carboxylate (5e)

Appearance - yellow compound; Yield – 58%; m.p. - 224-225 °C; FT-IR in cm⁻¹: 3421, 1679, 1587, 1506, 698; ¹H-NMR (400 MHz, CDCl₃); δ = 9.34-9.33 (1H, d, *J* = 6.8Hz), 8.37 (1H, s), 8.19 (1H, s), 7.66-7.60 (4H, m), 7.33 (1H, s), 4.45-4.41 (2H, q, *J* = 7.2Hz), 2.26 (3H, s), 1.46-1.44 (3H, t, *J* = 7.2Hz); ¹³C-NMR (100 MHz, CDCl₃); δ = 186.58, 164.72, 148.72, 139.45, 138.88, 137.53, 131.95, 130.97, 130.55, 127.75, 127.13, 123.39, 119.51, 110.61, 106.99, 60.08, 29.69, 14.51; MS (ESI Positive): HRMS (ESI-TOF) (m/z): [M+H]⁺ calculated for C₂₀H₁₇BrN₂O₄, 429.0372; found, 429.0493.

2.4.6. Ethyl (E)-3-(4-fluorobenzoyl)-7-((hydroxyimino)methyl)-2-methylindolizine-1-carboxylate (5f)

Appearance - yellow compound; Yield – 49%; m.p. - 201-202 °C; FT-IR in cm⁻¹: 3328, 2985, 1699, 1602, 1523, 1506, 1454, 1421, 1213; ¹H-NMR (400 MHz, CDCl₃); δ = 9.20-9.18 (1H, d, *J* = 6.8Hz), 8.24 (1H, s), 8.08 (1H, s), 7.68-7.65 (2H, m), 7.24-7.23 (1H, m), 7.11-7.07 (2H, m), 4.35-4.30 (2H, q, *J* = 7.2Hz), 2.15 (3H, s), 1.36-1.33 (3H, t, *J* = 7.2Hz); ¹³C-NMR (100 MHz, CDCl₃); δ = 186.46, 166.58, 164.85, 164.06, 148.51, 138.83, 137.39, 136.76, 136.73, 132.79, 131.87, 131.78, 131.67, 131.58, 130.98, 127.73, 125.73, 123.48, 119.42, 116.12, 115.94, 115.90, 115.72, 110.52, 109.72, 106.83, 60.46, 29.70, 14.86; HRMS (ESI-TOF) (m/z): [M+H]⁺ calculated for C₂₀H₁₇FN₂O₄, 369.1172; found, 369.1359.

2.4.7. Methyl (E)-3-(4-bromobenzoyl)-7-((hydroxyimino)methyl)-2-phenylindolizine-1-carboxylate (5g)

Appearance - brown compound; Yield – 62%; m.p. - 189-190 °C; FT-IR in cm⁻¹: 3371, 2923, 1681, 1612, 1583, 1527, 1469, 1429, 688; ¹H-NMR (400 MHz, CDCl₃); δ = 9.40-9.38 (1H, d, *J* = 6.8Hz), 8.35 (1H, s), 8.14 (1H, s), 7.35-7.31 (1H, m), 7.17-7.11 (2H, m), 7.06-6.94 (m, 7H), 3.62 (3H, s); ¹³C-NMR (100 MHz, CDCl₃); δ = 187.15, 164.54, 148.33, 140.60, 138.62, 137.75, 137.16, 133.27, 133.02, 132.68, 131.68, 131.12, 130.90, 130.60, 128.59, 127.97, 127.47, 127.10, 126.72, 126.22, 123.02, 119.86, 111.26, 110.46, 106.03, 51.12; HRMS (ESI-TOF) (m/z): [M+H]⁺ calculated for C₂₄H₁₇BrN₂O₄, 477.0372; found, 477.0529.

2.4.8. Methyl (*E*)-3-(4-fluorobenzoyl)-7-((hydroxyimino)methyl)-2-phenylindolizine-1-carboxylate (5h)

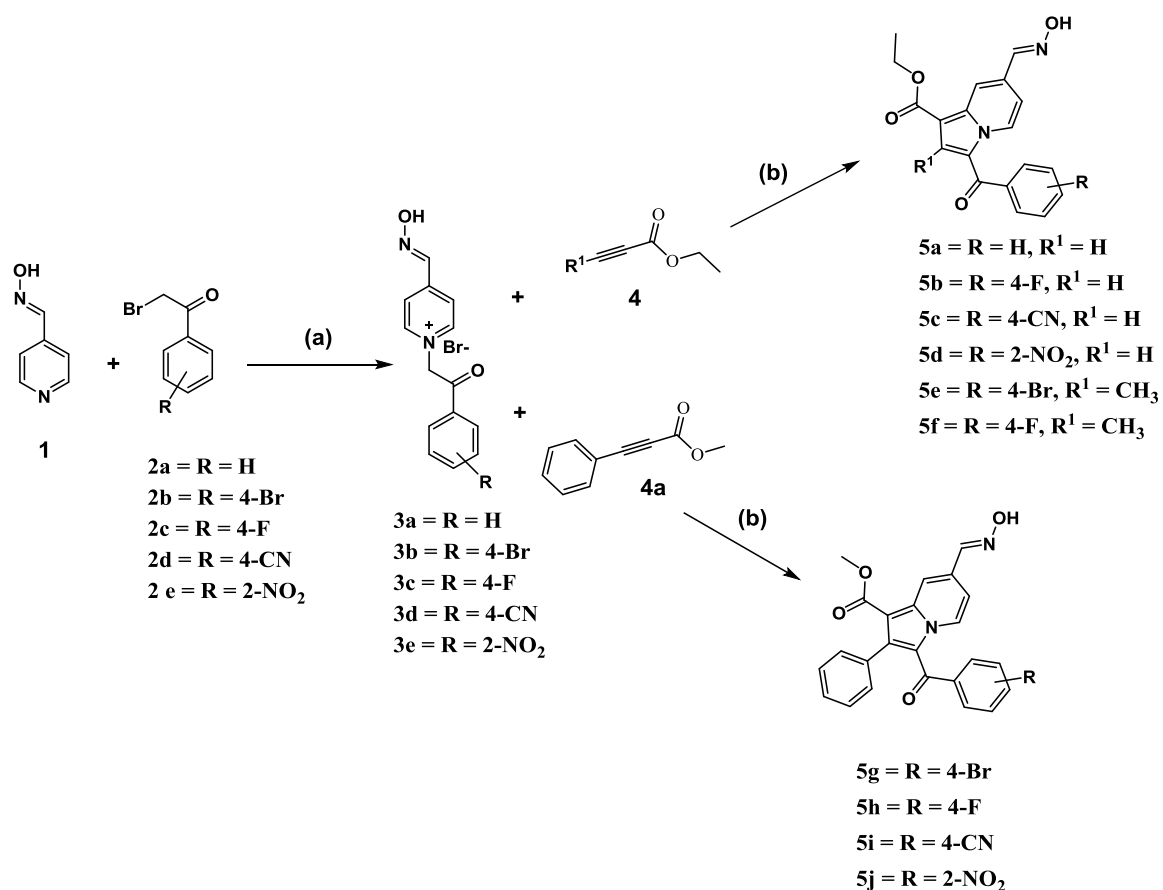
Appearance - yellow compound; Yield – 55%; m.p. - 159-160 °C; FT-IR in cm^{-1} : 3326, 3064, 2948, 1681, 1618, 1596, 1523, 1500, 1448, 1415, 1217; $^1\text{H-NMR}$ (400 MHz, CDCl_3); δ = 9.34-9.32 (1H, d, J = 6.8Hz), 8.35 (1H, s), 8.15 (1H, s), 7.35-7.29 (3H, m), 7.02-6.95 (5H, m), 6.63-6.59 (2H, m), 3.63 (3H, s); $^{13}\text{C-NMR}$ (100 MHz, CDCl_3); δ = 186.88, 165.68, 164.59, 163.16, 148.42, 140.20, 138.51, 135.10, 135.08, 133.28, 131.89, 131.76, 131.28, 130.85, 128.85, 127.97, 127.86, 127.27, 127.05, 123.12, 119.91, 114.97, 114.51, 111.11, 105.87, 51.10; HRMS (ESI-TOF) (m/z): $[\text{M}+\text{H}]^+$ calculated for $\text{C}_{24}\text{H}_{17}\text{FN}_2\text{O}_4$, 417.1172; found, 417.1466.

2.4.9. Methyl (*E*)-3-(4-cyanobenzoyl)-7-((hydroxyimino)methyl)-2-phenylindolizine-1-carboxylate (5i)

Appearance - yellow compound; Yield – 52%; m.p. - 212-213 °C; FT-IR in cm^{-1} : 3375, 2923, 2364, 1706, 1649, 1604, 1531, 1465; $^1\text{H-NMR}$ (400 MHz, CDCl_3); δ = 9.57-9.55 (1H, d, J = 6.8Hz), 8.39 (1H, s), 8.16 (1H, s), 7.42-7.20 (5H, m), 7.03-6.92 (5H, m), 3.68 (3H, s); $^{13}\text{C-NMR}$ (100 MHz, CDCl_3); δ = 186.24, 164.29, 148.34, 143.07, 141.43, 138.99, 133.82, 132.54, 132.02, 131.35, 131.29, 129.34, 129.28, 129.24, 128.22, 128.16, 127.88, 127.33, 127.12, 126.01, 122.66, 119.86, 118.18, 114.97, 113.87, 111.02, 106.59, 51.19; HRMS (ESI-TOF) (m/z): $[\text{M}+\text{H}]^+$ calculated for $\text{C}_{25}\text{H}_{17}\text{N}_3\text{O}_4$, 424.1219; found, 424.1366.

2.4.10. Methyl (*E*)-7-((hydroxyimino)methyl)-3-(2-nitrobenzoyl)-2-phenylindolizine-1-carboxylate (5j)

Appearance - brown compound; Yield – 59%; m.p. - 197-198 °C; FT-IR in cm^{-1} : 3325, 1681, 1608, 1514, 1442, 1417; $^1\text{H-NMR}$ (400 MHz, CDCl_3); δ = 10.17-10.15 (1H, m), 8.87 (1H, s), 7.77-7.75 (1H, m), 7.47-7.40 (3H, m), 7.31-7.26 (3H, m), 7.05-6.88 (4H, m); $^{13}\text{C-NMR}$ (100 MHz, CDCl_3); δ = 184.67, 163.31, 145.47, 142.07, 136.47, 136.27, 133.64, 132.30, 130.04, 129.31, 129.18, 129.02, 128.87, 128.64, 128.40, 128.28, 127.66, 127.24, 125.84, 124.17, 123.02, 117.26, 115.39, 110.47, 108.90, 51.45; HRMS (ESI-TOF) (m/z): $[\text{M}+\text{H}]^+$ calculated for $\text{C}_{24}\text{H}_{17}\text{N}_3\text{O}_6$, 444.1117; found, 444.1370.



Scheme 1: Synthetic scheme of (*E*)-1-(2-(4-substituedphenyl)-2-oxoethyl)-4-((hydroxyimino)methyl)pyridinium compounds **3a-3e**, (*E*)-3-(substituedbenzoyl)-7-((hydroxyimino)methyl)-2-substitutedindolizine-1-carboxylate compounds **5a-5f** and methyl (*E*)-7-((hydroxyimino)methyl)-3-(substituedbenzoyl)-2-phenylindolizine-1-carboxylate compounds **5g-5j**. Reaction conditions (a) Dry acetone, stir, room temperature, 30 min; (b) DMF, stir, room temperature, 30 min.

2.5. Crystallography Data Collection, Structure Solution and Refinement

Single-crystal X-ray diffraction data were collected on a Bruker KAPPA APEX II DUO diffractometer using graphite monochromated Mo K α radiation ($\lambda = 0.71073 \text{ \AA}$). Data collection (36) was carried out at 100(2) K. Temperature was controlled by an Oxford Cryostream cooling system (Oxford Cryostat). Cell refinement and data reduction were performed using the program SAINT (37). The data were scaled, and absorption correction was performed using SADABS (37). Single crystal X-ray data and refinement parameters of compounds **3a** and **5f** are tabulated in Table 1.

The structure was solved via direct methods using SHELXS-97 (38) and refined via the full-matrix least-squares method based on F^2 using SHELXL-2014 (39). All non-hydrogen atoms were refined anisotropically. The hydrogen atoms of the hydroxyl group and water molecule were initially located from a difference Fourier Map. All the other hydrogen atoms, connected to carbon atoms, were placed in idealized positions and refined in riding models with U_{iso} assigned 1.2 or 1.5 times the U_{eq} of their parent atoms. All the geometrical calculations were done using PLATON (40). The programs WinGx (41) and Mercury (42) were used to prepare the molecular graphic images.

2.6. Anti-tubercular Screening: Resazurin Microplate Assay (REMA)

The biological activities of compounds **3a-3i** and **5a-5j** were assessed using the colorimetric REMA plate approach as detailed previously (23, 43). Briefly, the minimum inhibitory concentration (MIC) of the tested compounds was determined using the agar incorporation approach and performed in triplicates against H37Rv, MDR of MTB. The targeted strains were cultured in Middlebrook 7H11 medium for 3 weeks (44). Then, the bacterial strains were incubated at 37 °C and then standardized to obtain a bacterial concentration of $\sim 1 \times 10^7$ cfu/mL. Finally, a 100 μ L of diluted bacterial suspension with drug doses ranging from 128–0.125 μ g/mL was poured onto Middlebrook 7H10 agar plates and were incubated for 3 weeks, after which the MICs of the tested compounds were obtained. MDR clinical isolates were resistant to isoniazid and rifampicin.

2.7. InhA Inhibition Assay

Triclosan and NADH were purchased from Alfa Aesar. Stock solutions of all compounds were prepared in DMSO such that the final concentration of DMSO was constant at 5% v/v in a final volume of 1 mL for all kinetic reactions. Kinetic assays were performed using purified *trans*-2-dodecenoyl-coenzyme A (DDCoA) and wild-type InhA as previously described (45, 46). Briefly, reactions were performed at 25 °C in the buffer (30 mM PIPES and 150 mM NaCl at pH 6.8) containing 250 μ M NADH, 50 μ M substrate (DDCoA), and the tested compounds **3a-3i** and **5a-5j** (at

50 μM and/or 5 μM). Reactions were initiated by adding the enzyme InhA (50 nM final), and NADH oxidation was followed at 340 nm. The initial velocity of the reaction (v) was established with respect to the velocity of the control reaction without inhibitor (v_0). The inhibitory activity of each compound was expressed as the percentage inhibition of InhA activity $(1-v/v_0) \times 100\%$. Triclosan (TCL) was used as a positive control. All activity assays were performed in duplicate or triplicate, depending on the inhibitory activity.

2.8 Computational Materials

ChemBioDraw Ultra 12 was used to sketch the 2D chemical structure of the tested compound, which were then imported into Discovery Studio (DS) 2017 (BIOVIA, Dassault Systèmes, Discovery Studio, 2017, San Diego: Dassault Systèmes, 2017) for further processing and preparation. DS was utilized to run all computational procedures. Generated images were prepared using PyMol molecular graphics system (47) and DS.

2.8 Computational Methods

In this study, the same *in silico* approach that we previously implemented (34, 35) to identify putative MTB targets for a set of compounds was utilized (Figure 1). In this approach, an extensive literature survey had revealed 20 essential mycobacterial drug targets with available 3D structures that were used as structural models for molecular docking studies. The crystal structures of those 20 essential MTB targets were downloaded from the Protein Data Bank (PDB) and prepared using DS by correcting connectivity and bond order, standardizing atom names, and protonating them at a pH of 7.4; then, they were solvated and minimized, and they were ready for further modeling steps. Then, the tested compounds (**3a-3e** and **5a-5j**) were prepared by assigning proper bond order and generating different tautomers and ionization states and docked into the active site of each of those 20 essential MTB enzymes using the CDOCKER algorithm in DS. The docked compounds were then rescored with different scoring functions, and their Pearson correlation coefficients with the experimental MIC values were calculated. The enzymes that showed the highest correlation values were deemed putative targets for the tested compounds. Moreover, different pharmacokinetic and toxicity parameters for the tested compounds were calculated using the ADMET Descriptors protocol and the Toxicity Prediction (TOPKAT) protocol in DS.

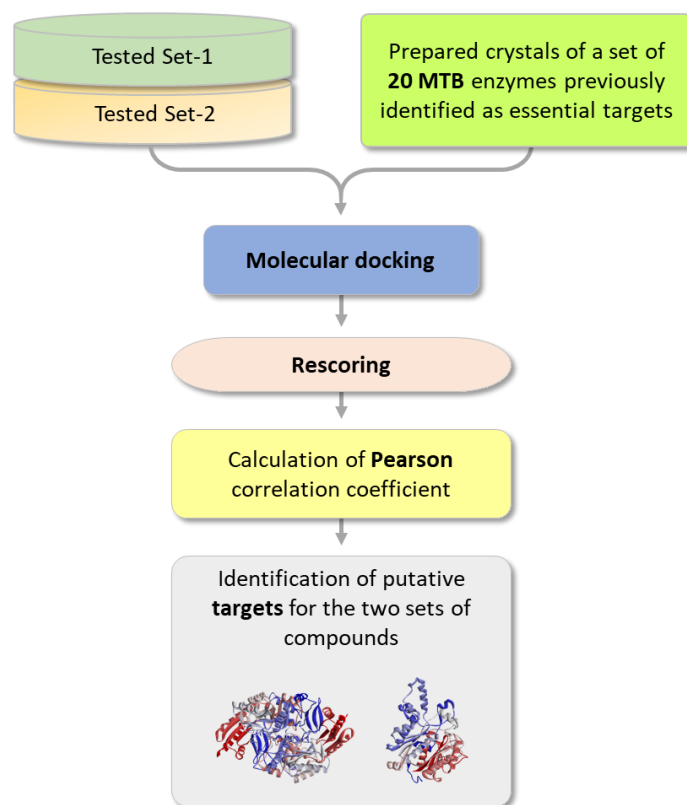


Figure 1. Summary of the computational workflow implemented in this study.

3. Results and Discussion

3.1 Chemistry

The synthesis of the first set of compounds (*E*)-1-(2-(substitutedphenyl)-2-oxoethyl)-4-((hydroxyimino)methyl)pyridin-1-ium bromides (**3a-e**) was achieved by a reaction between 4-pyridine aldoxime (**1**) and substituted phenacyl bromide (**2a-e**) in the presence of dry acetone. The resulting compounds (**3a-e**) were treated with ethyl propiolate (**4a**), ethyl but-2-ynoate (**4e**), and ethyl 3-phenylpropiolate (**4g**) to obtain title compounds **5a-d**, **5e-f** and **5g-j**, respectively as depicted in Scheme 1. The completion of the reaction was monitored by TLC, and the product was purified by column chromatography using hexane and ethyl acetate as an eluent. The purified compounds were characterized by spectroscopic techniques, and the structures of the compounds were confirmed by FT-IR, ¹H-NMR, ¹³C-NMR, LC-MS, and elemental analysis. A probable reaction mechanism for the construction of ethyl (*E*)-3-benzoyl-7-((hydroxyimino)methyl)indolizine-1-carboxylate (**5a**) is illustrated in Figure 3. The quaternary ammonium salt (**3a**) in the presence of solvent and base (potassium carbonate) generates an anion (I). This reactive anion undergoes a reaction with electron-deficient ethyl propiolate (**4a**), then the migration of the alkyne bond of ethyl propiolate carbanion takes place and add to the carbocation of the compound (**3a**), and it will give an

intermediate (II). The intermediate (II) will undergo aromatization *via* oxidation in dry DMF to yield an indolizine nucleus in ethyl (*E*)-3-benzoyl-7-((hydroxyimino)methyl)indolizine-1-carboxylate (**5a**).

The synthesis of the two sets of title compounds **3a-e** and **5a-j** against MTB is depicted in Scheme 1. These compounds were synthesized in two-step chemical synthetic methods. In the initial step, the 4-pyridine aldoxime was mixed with substituted phenacyl bromides in the presence of acetone solvent; the obtained products were filtered and dried under a vacuum. The obtained quaternary salts were treated with electron-deficient alkynes in the presence of a potassium carbonate base with anhydrous DMF. The completion of the reaction was monitored by TLC. After the reaction completion, the product was purified by column chromatography using hexane and ethyl acetate as an eluent. The purified compounds were characterized by spectroscopic methods. The structures of the compounds were confirmed by FT-IR, ¹H-NMR, ¹³C-NMR, LC-MS, and elemental analysis. A probable reaction mechanism for the construction of ethyl (*E*)-3-benzoyl-7-((hydroxyimino)methyl)indolizine-1-carboxylate (**5a**) is illustrated in Figure 2.

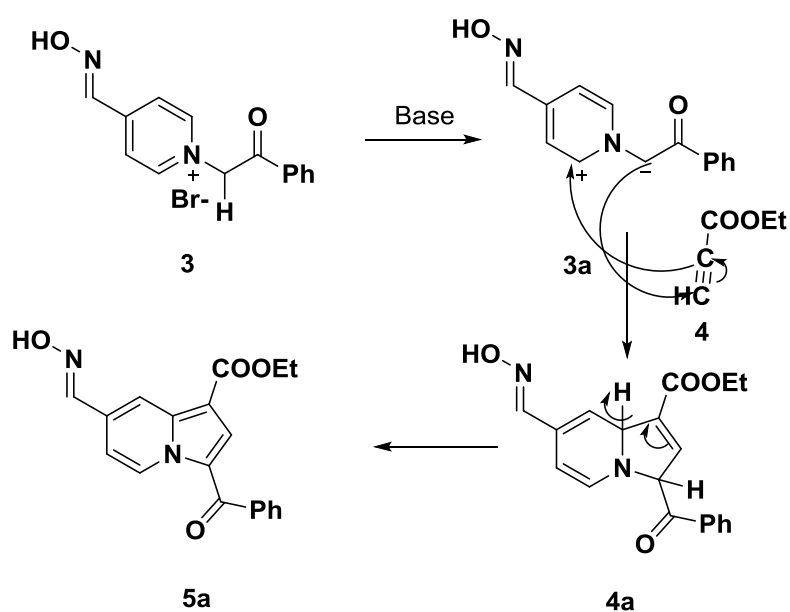


Figure 2: Probable reaction mechanism for the construction of (*E*)-3-(substitutedbenzoyl)-7-((hydroxyimino)methyl)-2-substitutedindolizine-1-carboxylate derivatives (**5a-5j**)

3.2. Crystallography

Crystal Packing Analysis of Compound **3a**

This compound (**3a**) crystallizes in the monoclinic $P2_1/n$ centrosymmetric space group with one molecule of the compound along with the bromide ion as a counter ion and one molecule of water [Figure 3a]. The asymmetric unit is stabilized via O-H...Br⁻ (involving H3B and Br1) and C-H...Br⁻ (involving H3 and Br1) hydrogen bonds. A tetrameric square motif consisting of two water molecules

and two bromide ions held via O-H...Br⁻ H-bonds (involving H3A, H3B with Br1) are formed, and the oxygen atoms of water molecules are connected via O-H...O H-bonds, involving the hydroxyl group on the molecule with the oxygen atom of the water molecule in a centrosymmetric manner. The bromide ions are connected via C-H...Br⁻ H-bonds, involving H8A and Br1, again in a centrosymmetric manner. Two such adjacent tetrameric motifs are connected to each other via C-H...O H-bonds, involving H4 and O1 [Figure 4] forming an octameric motif. Furthermore, there exists C-H...N, C-H...O and C-H...Br intermolecular interactions that provide additional stability to the crystal lattice [Table 2].

Crystal Packing Analysis of Compound 5f

The molecule crystallizes in the monoclinic non-centrosymmetric space group *Cc* with one molecule in the asymmetric unit [Figure 3b]. The molecular conformation is locked via C-H...O intramolecular H-bonds. The molecules are held via O-H...O (involving H1 and O4) and C-H...N (involving H16 and N2), forming chains via the *c*-glide operation along the *z*-axis [Figure 5, Table 3]. These are further stabilized via C-H...F H-bonds (involving H4, H5 with F1), along with C-H...O H-bonds (involving H1C, H7, and O1) wherein both oxygen atom O1 and fluorine atom F1 functions as a bifurcated acceptor.

Table 1: Single crystal X-ray data and refinement parameters of compounds **3a** and **5f**.

Compounds code	3a	5f
CCDC number	2024681	2024679
Molecular formula	C14 H15 Br N2 O3	C20 H17 F1 N2 O4
Molecular weight	339.19	368.35
Temperature	100(2)	100(2)
Crystal size (mm)	0.120×0.11×0.090	0.22×0.05×0.04
Absorption coefficient (mm ⁻¹)	2.879	0.106
T _{min} , T _{max}	0.724, 0.782	0.977, 0.996
Crystal system	Monoclinic	Monoclinic
Lattice parameters: a (Å), b (Å), c (Å)	7.8323(3), 15.0173(6), 12.2646(6)	4.7923(5), 30.196(4), 12.0372(15)
α, β, γ(°)	90, 96.991(2), 90	90, 91.125(4), 90
Space group, Density, Z, Z'	<i>P</i> 2 ₁ / <i>n</i> , 4, 1	<i>Cc</i> , 4, 1
h _{min} , max; k _{min} , max; l _{min} , max;	-10, 10; -20, 20; -16, 16	-5,5;-37,37;-15,15
Number of unique/observed data	3557/2929	3506, 2774
No of parameters	193	297

R_{int}	0.0544	0.1511
$R_{\text{all}}, R_{\text{obs}}$	0.0448, 0.0285	0.1422, 0.1131
$wR2_{\text{all}}, wR2_{\text{obs}}$	0.0748, 0.0638	0.2450, 0.2320
$\Delta\rho_{\text{min/max}}$ ($\text{e}\text{\AA}^{-3}$)	0.559, -0.444	0.354, -0.329
G.o.F	1.129	1.107

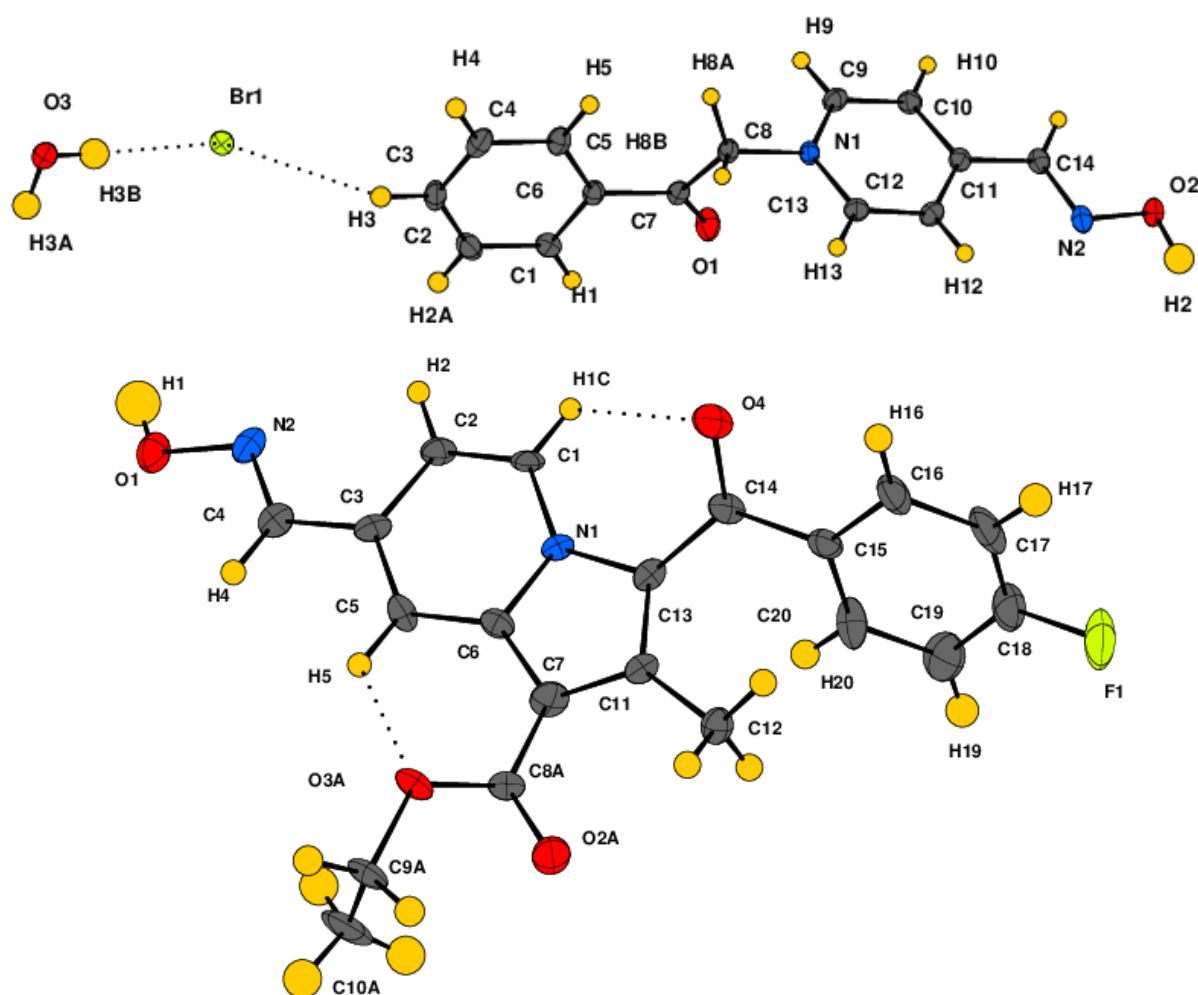


Figure 3: ORTEP drawn at 50% ellipsoidal probability for a) compound **3a** and b) compound **5f**. The dotted lines indicate intra- and intermolecular contacts in the asymmetric unit.

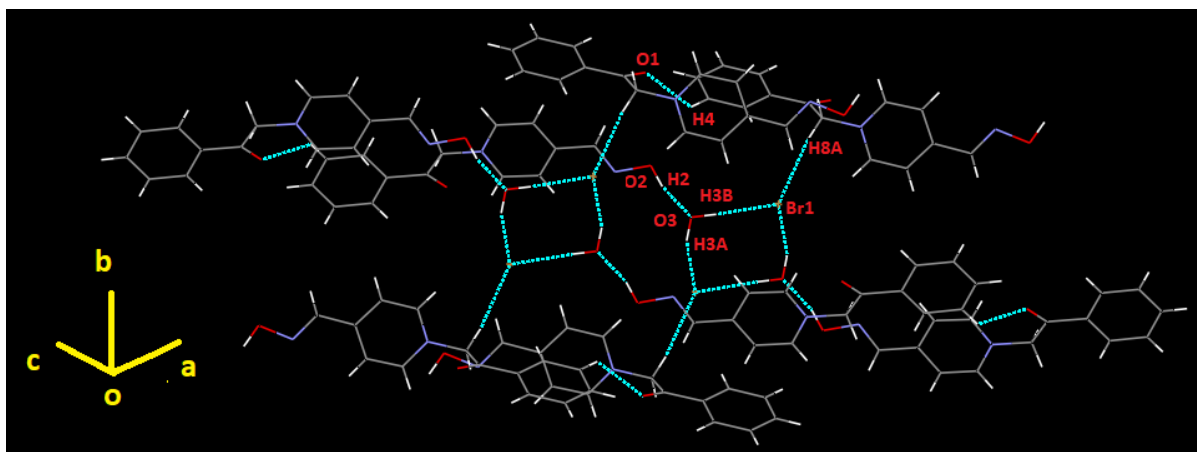


Figure 4: Packing diagram of compound **3a**. The blue dotted lines depict intermolecular interactions.

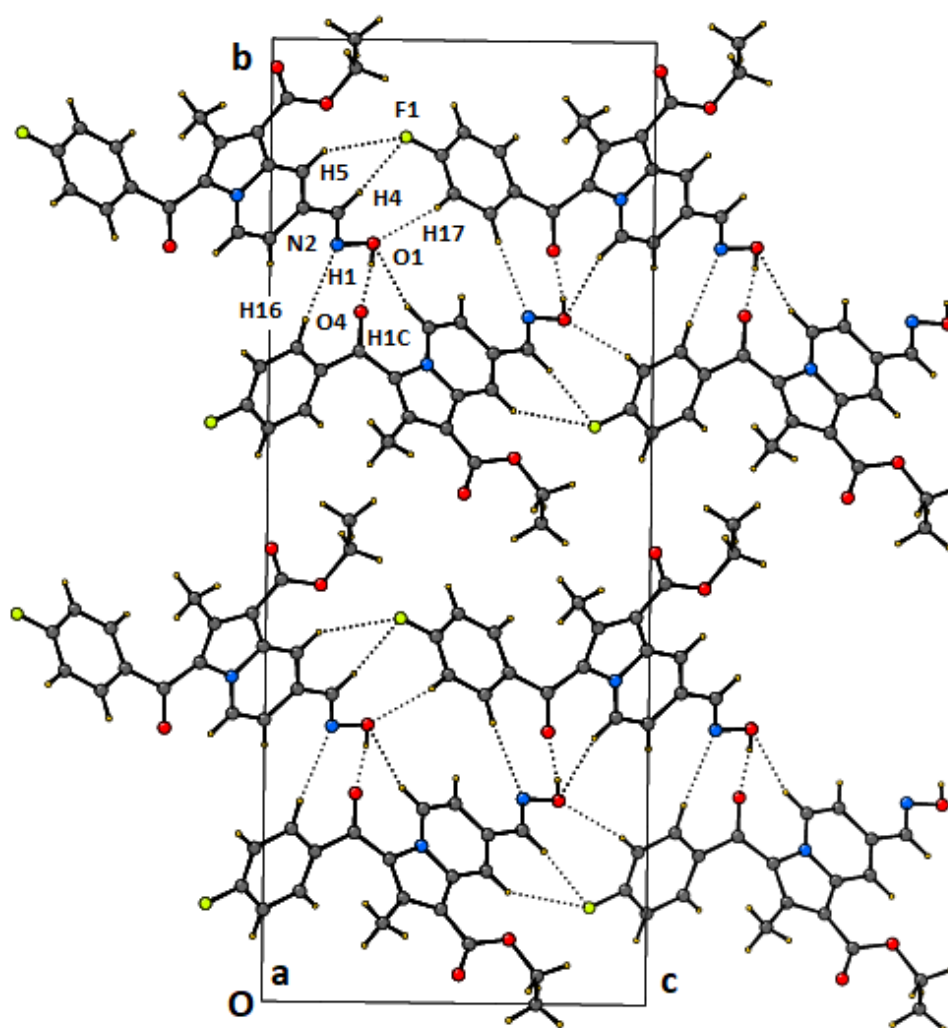


Figure 5: Packing diagram of compound **5f** down the *a*-axis. The dotted lines depict intermolecular interactions.

Table 2: List of intra- and intermolecular interactions in the crystal structures of compounds **3a** and **5f**.

Interaction Type	D-H (Å)	D...A (Å)	H...A (Å)	D-H...A (°)	Symmetry code
Compound 3a					
O3-H3B...Br1	0.96	3.294	2.34	172	x, y, z
C3-H3...Br1	0.95	3.825	2.95	153	x, y, z
O2 -H2...O3	0.97	2.623	1.67	166	x+2,+y,+z-1
O3-H3A...Br1	0.96	3.291	2.39	157	-x,-y+1,-z+2
C2-H2A...N2	0.95	3.649	2.74	160	-x+2,-y+1,-z+1
C4-H4 ...O1	0.95	3.305	2.60	132	x-1,+y,+z
C4-H4...O2	0.95	3.431	2.66	139	x-3/2,-y+1/2,+z+1/2
C8-H8A...Br1	0.99	3.662	2.68	172	x+1/2,-y+1/2,+z-1/2
C9-H9...O2	0.95	3.334	2.71	124	x-1/2,-y+1/2,+z+1/2
C10-H10...O3	0.95	3.476	2.75	134	x+3/2,-y+1/2,+z-1/2
C13-H13...Br1	0.95	3.736	2.95	141	-x+1,-y+1,-z+1
C12-H12...O3	0.95	3.810	2.87	173	-x+1,-y+1,-z+1
Compound 5f					
C1-H1C...O4	0.95	2.867	2.30	118	x, y, z
C5-H5...O3A	0.95	2.896	2.40	112	x, y, z
O1-H1 ...O4	0.85	2.699	1.86	171	x+3/2,-y+3/2,+z+1/2
C1-H1C...O1	0.95	3.447	2.67	139	x-1/2,-y+3/2,+z-1/2
C5-H5...F1	0.95	3.440	2.61	147	x+1,+y,+z+1
C4-H4...F1	0.95	3.574	2.79	141	x+1,+y,+z+1
C16-H16...N2	0.95	3.559	2.62	172	x-3/2,-y+3/2,+z-1/2
C17-H17...O1	0.95	3.407	2.52	156	x-2,+y,+z-1

3.3. Pharmacology

3.3.1. *In vitro* Bacterial Growth Inhibition Experiment

The *in vitro* inhibitory activity of the tested compounds (**3a-3e** and **5a-5j**) against H37Rv (ATCC: 25177) and MDR strains of MTB are presented in Table 3. Triclosan, streptomycin, and isoniazid were used for comparison. Among (*E*)-1-(2-(4-substitutedphenyl)-2-oxoethyl)-4-((hydroxyimino)methyl)pyridinium derivatives (**3a-3e**), the compound **3d** exhibited significant inhibitory activity against the H37Rv strain of MTB with MIC value of 16 µg/mL, but it showed weak inhibitory activity against the MDR strain with MIC value of 128 µg/mL. Whereas compounds **3a-3c**

and **3e** showed moderate inhibitory activities against the H37Rv and MDR strains of MTB with MIC values ranging from 16-64 µg/mL and 64-128 µg/mL, respectively. Among ethyl-(*E*)-3-substitutedbenzoyl-7-((hydroxyimino)methyl)indolizine-1-carboxylate derivatives (**5a-5d**), compound **5a** with unsubstituted benzoyl group showed same activity as compound **5c** with 4-cyanobenzoyl against H37Rv and MDR strains of MTB with MIC values of 8 µg/mL and 16 µg/mL, respectively. The presence of electron-withdrawing fluorine (F) atom at the para-position of benzoyl moiety of compound **5b** showed better activity against H37Rv (MIC 10 µg/mL) and MDR (MIC 20 µg/mL) strains of MTB as compared to compound **5d** having electron-withdrawing nitro group at the 2-position of benzoyl group exhibiting MIC values of 16 µg/mL and 64 µg/mL against H37Rv and MDR strains of MTB, respectively. Among ethyl-(*E*)-3-substitutedbenzoyl-7-((hydroxyimino)methyl)-2-methylindolizine-1-carboxylate derivatives (**5e-5f**), compound **5e** with stronger electron-withdrawing bromine (Br) atom attached to the 4-position of benzoyl group exhibited excellent inhibitory activity against the H37Rv (MIC 6 µg/mL), but moderate activity against the MDR strain (MIC 64 µg/mL) of MTB, as compared to compound **5f** with 4-fluorobenzoyl moiety exhibiting MIC values of 11 µg/mL and 32 µg/mL against H37Rv and MDR strains, respectively.

In case of methyl-(*E*)-3-(4-substitutedbenzoyl)-7-((hydroxyimino)methyl)-2-phenylindolizine-1-carboxylates (**5g-5j**), compound **5h** was found to be the most potent against H37Rv (MIC 5 µg/mL) and MDR (MIC 16 µg/mL) strains of MTB as compared to all other compounds. Interestingly, the presence of electron-withdrawing group at the 4-position of benzoyl group also resulted in potential inhibitory activities against both strains of MTB for the compounds **5g** containing 4-bromobenzoyl (MIC, H37Rv = 12 µg/mL and MDR = 32 µg/mL) and **5i** 4-cyanobenzoyl group (MIC, H37Rv = 8 µg/mL and MDR = 16 µg/mL), respectively. However, the attachment of the electron-withdrawing nitro (NO₂) group at the 2-position of the benzoyl group resulted in a slight decrease in activities in compound **5j** with MIC values of 16 µg/mL against both strains of MTB.

3.3.2. *In vitro* InhA Inhibition Assay

Previously, we designed a series of compounds and tested them against the mycobacterial InhA enzyme (48, 49), and since we have a well-established bioassay against this enzyme in our lab, we decided to test the inhibitory activities of the two newly synthesized sets (**3a-3e** and **5a-5j**) against this enzyme hoping their mechanism of action will be revealed.

Therefore, all compounds (**3a-3e**, and **5a-5j**) were investigated (*in vitro*) for their inhibitory activity against InhA from MTB at 50 µM (and/or at 5 µM) by applying our previously reported method (48, 49). Recombinant MTB InhA was expressed using *E. coli* and subsequently purified with little modification based on the previously reported procedure. Triclosan was tested for comparison at

the same concentration and showed complete inhibition at 10 μ M. The results of the percentage inhibition of InhA are presented in Table 3.

Among (*E*)-1-(2-(4-substitutedphenyl)-2-oxoethyl)-4-((hydroxyimino)methyl)pyridinium derivatives (**3a-3e**), the compounds **3b** and **3d** with 4-bromophenyl and 4-cyanophenyl group, respectively exhibited good inhibitory activities with 10% and 17% inhibition of InhA activity, respectively. Compounds **3a** and **3e** with unsubstituted phenyl ring and 2-nitrophenyl ring showed weak inhibition of InhA (5%). Compound **3d** exhibited better inhibitory activity against both H37Rv as well as InhA as compared to the similar analogs **3a-3c** and **3e**.

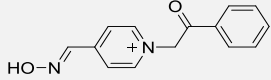
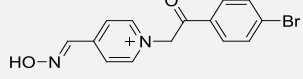
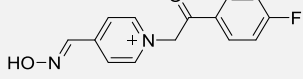
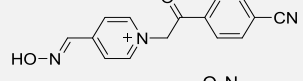
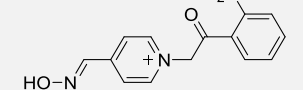
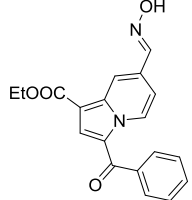
The compound **3a** with unsubstituted-benzoyl group attached to the pyridinium moiety showed poor InhA inhibitory activity (5% at 50 μ M), but the conversion of pyridinium ring into 1-ethylcarboxylate-indolizine group containing unsubstituted-benzoyl group resulted in compound **5a** with increased InhA inhibitory activity (10% at 50 μ M). A similar trend was also observed in compounds containing the 4-bromophenyl group (**3b**, **5e**, and **5g**) and the 4-fluorophenyl group (**3c**, **5b**, **5f**, and **5h**). Compound **3b**, with a 4-bromophenyl group attached to the pyridinium moiety, showed moderate InhA inhibitory activity (10% at 50 μ M). Whereas compound **5e** with a methyl group attached to the 2-position of the indolizine group containing 1-ethylcarboxylate and 4-bromobenzoyl groups, and compound **5g** with a phenyl group attached to the 2-position of the indolizine group containing 1-methylcarboxylate and 4-bromobenzoyl groups showed increased activities with 20% and 19% inhibition of InhA, respectively, as compared to the compound **3b**. It is interesting to note that compound **3c** with 4-fluorobenzoyl group attached to the pyridinium moiety did not show any activity against InhA, whereas the conversion of the pyridinium ring into indolizine group having 1-ethylcarboxylate group resulted in compound **5b** with moderate inhibitory activity against InhA (11%). The addition of methyl group to the 2-position of indolizine group containing 1-ethylcarboxylate and 4-fluorobenzoyl groups resulted in the most potent compound of the series, **5f**, exhibiting 52% and 33% inhibition of InhA at 50 μ M and 5 μ M, respectively. However, the replacement of 1-ethylcarboxylate with 1-methylcarboxylate group and 2-methyl with a 2-phenyl group in indolizine moiety containing 4-fluorobenzoyl groups caused a slight decrease in the activity, as evident from compound **5h** (35% inhibition of InhA at 50 μ M).

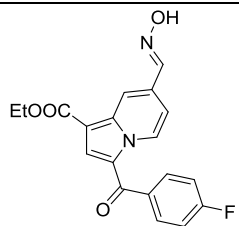
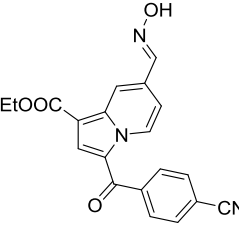
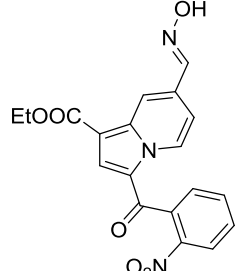
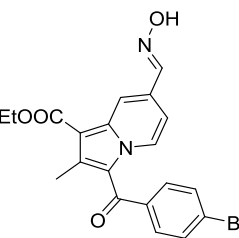
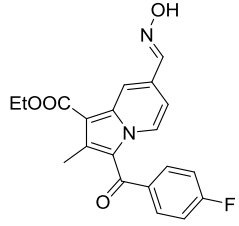
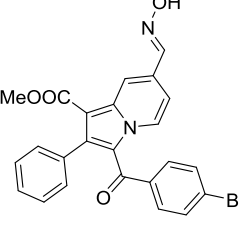
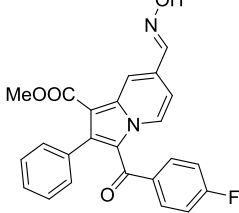
Compound **3d** with a 4-cyanophenyl group attached to the pyridinium moiety exhibited better inhibitory activity against InhA (17% at 50 μ M) as compared to the similar (*E*)-1-(2-(4-substitutedphenyl)-2-oxoethyl)-4-((hydroxyimino)methyl)pyridinium analogues (**3a-3c** and **3e**). However, converting the pyridinium ring into 1-ethylcarboxylate-indolizine group containing a 4-cyanophenyl group resulted in compound **5c** with no InhA inhibitory activity as observed at 50 μ M.

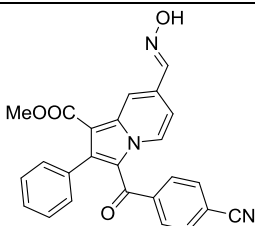
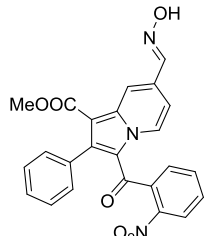
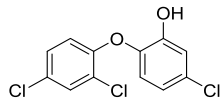
But the replacement of 1-ethylcarboxylate with 1-methylcarboxylate group and addition of a phenyl group at the 2-position of the indolizine core resulted in the second most potent compound **5i** with 48% and 29% inhibition of InhA at 50 μ M and 5 μ M, respectively. Compound **5d** containing 1-ethylcarboxylate and 2-nitrobenzoyl groups attached to the indolizine core showed five times increased inhibitory activity (25% inhibition) as compared to the compound **3e** with 2-nitrobenzoyl group attached to the pyridinium moiety (5% inhibition) against InhA at 50 μ M. Whereas the replacement of 1-ethylcarboxylate with 1-methylcarboxylate group and addition of a phenyl group at the 2-position of the indolizine core resulted in a drastic reduction in activity for compound **5j** with <5% InhA inhibition at 50 μ M.

Unfortunately, there was no clear correlation between the InhA inhibitory activity of the tested compounds and their MIC values against whole-cell MTB strains, which indicates that they might have different modes of action other than InhA inhibition. Therefore, a computational investigation was conducted by employing molecular docking aiming to identify their putative drug target(s), accordingly, understand their mechanism of action.

Table 3: Minimum Inhibitory Concentration (MIC) values against H37Rv and MDR strains of *M. tuberculosis*, and InhA inhibition values of (*E*)-1-(2-(4-substitutedphenyl)-2-oxoethyl)-4-((hydroxyimino)methyl)pyridinium derivatives (**3a-3e**) and (*E*)-3-(substitutedbenzoyl)-7-((hydroxyimino)methyl)-2-substitutedindolizine-1-carboxylate derivatives (**5a-5j**).

Compounds Code	Chemical Structure	MIC (μ g/mL)		% Inhibition of InhA ^a at 50 μ M (5 μ M)
		Susceptible (H37Rv)	MDR-TB	
3a		32	64	5
3b		32	64	10
3c		32	128	NI ^b
3d		16	128	17
3e		64	64	5
5a		8	16	10

5b		10	20	11
5c		8	16	NI ^b
5d		16	64	25
5e		6	64	20
5f		11	32	52 (33)
5g		12	32	19
5h		5	16	35

5i		8	16	48 (29)
5j		16	16	<5
Triclosan (TCL)		20	NT ^c	97
Streptomycin		0.25	NT	---
Isoniazid (INH)		0.025	NT	---

^a All activity assays were performed in duplicate or triplicate (when inhibitory activity).

^b NI for no inhibition at the given concentration.

^c NT for not tested.

3.4. Computational Modeling Studies

3.4.1 Identification of Putative Drug Targets for the Tested Compounds

Contrary to the previous anti-mycobacterial drug discovery methods, which mostly focused on biochemical and target-based inhibitor screens that, unfortunately, had not resulted in any new TB drugs, recent efforts were shifted to developing whole-cell screening assays. Since MTB encounters complex microenvironments within the human host, different screening methods that better mimic the *in vivo* conditions of MTB inside the bodies of TB patients have been developed (50). With whole-cell screening methods, the availability of a plethora of potential drug targets within MTB cells complicates the identification of specific targets for identified hits that could be responsible for their observed activity. Yet, the specific mycobacterial drug target for that hit needs to be identified in order to aid more rational prospective lead optimization efforts.

In this study, the whole-cell screening method was used to evaluate the anti-tubercular activities of the tested compounds. Further, they were tested (*in vitro*) against the InhA enzyme; unfortunately, the results were not correlated with the whole-cell screening MIC values. Therefore, implementing computational methods sought to identify putative drug targets that could explain the mechanism of

action of the tested compounds. The same approach we used previously (34, 35) was used in this study, based on an exhaustive literature review to identify known essential and potential MTB drug targets. Then, 20 targets with solved 3D structures were selected as structural models for molecular docking studies (35) (Table 4).

Table 4: The selected 20 essential mycobacterial drug targets for molecular modeling studies.

Index	MTB Protein Target	Targeted pathway	PDB ID	References
1	Decaprenylphosphoryl- β -d-ribofuranose oxidoreductase (DprE1)	Cell wall biosynthesis: arabinogalactan biosynthesis	4P8C	(51-53)
2	Enoyl-ACP-reductase, (InhA)	Cell wall biosynthesis: mycolic acid biosynthesis	6R9W	(54)
3	Mycolic acid cyclopropane synthase (CmaA2)	Cell wall biosynthesis: mycolic acid biosynthesis	1KPI	(55)
4	β -ketoacyl acyl carrier protein synthase I (KasA)	Cell wall biosynthesis: mycolic acid biosynthesis	6P9L	(56)
5	Polyketide synthase (Pks13)	Cell wall biosynthesis: mycolic acid biosynthesis	5V3Y	(57, 58)
6	Enoyl-CoA hydratase 6 (EchA6)	Cell wall biosynthesis: mycolic acid biosynthesis	5DUF	(59)
7	Transcriptional repressor of EthA monooxygenase (EthR)	Cell wall biosynthesis: mycolic acid biosynthesis (indirect)	5EYR	(60)
8	Alanine racemase (alr)	Cell wall biosynthesis: peptidoglycan biosynthesis	1XFC	(61)
9	MurE (Mur Ligase family)	Cell wall biosynthesis: peptidoglycan biosynthesis	2WTZ	(62)
10	Bifunctional enzyme (GlmU)	Cell wall biosynthesis	2QKX	(63)
11	2-methylcitrate synthase (PrpC) or (GltA3)	Fatty acid biosynthesis	3HWK	(64)
12	3-oxoacyl-[acyl-carrier-protein] synthase 3 (FabH)	Fatty acid biosynthesis	1HZP	(56)
13	β -ketoacyl-ACP reductase (MabA)	Fatty acid biosynthesis	1UZN	(65)
14	Aspartyl-tRNA Synthetase (AspS)	Protein synthesis	5W25	(66)
15	Leucyl-tRNA synthase (LeuRS)	Protein synthesis	5AGS	(50)
16	Protein kinase B (PknB)	Signal transduction	5U94	(67)
17	Protein kinase A (PknA)	Signal transduction	6B2Q	(68)
18	Pantothenate kinase (PanK, type 1)	Cofactor biosynthesis: Coenzyme A biosynthesis	4BFZ	(69)
19	Pyridoxal-5'-phosphate (PLP)-dependent aminotransferase (BioA)	Cofactor biosynthesis: biotin biosynthesis	4XJO	(70)

20	Aspartate aminotransferase (aspAT)	Asp biosynthesis, and Asp-dependent nitrogen metabolism	6U7A	(71)
----	------------------------------------	---	------	------

All selected crystal complexes were prepared as detailed previously (72, 73). Following crystal preparation, the binding sites were defined based on the co-crystallized ligands, after which the co-crystallized ligands were extracted and redocked into their respective binding sites to validate the docking protocol before docking the tested compounds. If the binding site is well-defined and the docking algorithm is accurate enough, then the orientation of the redocked pose should match that of the native co-crystallized ligand. Besides, the co-crystallized inhibitors were intended to be used as virtual positive controls during the docking studies (74). The redocking validation step was performed using the CDOCKER docking algorithm, which successfully reproduced the binding orientation of the co-crystallized ligands with RMSD values ranging from 0.2 to 1.43 Å.

Having been well-validated, the docking protocol was applied in docking the tested compounds into the active site of each selected MTB target. Out of the 20 selected enzymes, all compounds had failed to dock into the alanine racemase (alr) enzyme; similarly, compounds **5a-5j** had also failed to dock into the aspartyl-tRNA synthetase (AspS) enzyme.

Although CDOCKER is a well-validated docking algorithm, it is highly recommended to rescore the docked poses using other scoring functions so as to remediate any possible bias that might result from using a single scoring function (75). Generally, scoring functions fall into four classes, forcefield-based, empirical, knowledge-based, and machine-learning-based scoring functions (75). Therefore, in addition to the two CDOCKER forcefield based scores, the -CDOCKER energy (-CDE) and the -CDOCKER interaction energy (-CDIE), the docked poses were rescored using LigScore1 and LigScore2 (76), PLP1 (77) and PLP2 (78), and Jain (79), which are empirical scoring functions, in addition to another two knowledge-based scoring functions, PMF (80) and PMF04 (81). These scoring functions are available in DS, and their output scores are reported as positive values; hence, the higher the score, the higher the binding affinity.

To identify the putative target(s) for the tested compounds, we calculated the Pearson correlation coefficient (r) between their different computational scores and their respective experimentally determined MIC values. The r measures the strength of linear association between two variables, and it can take a range of values from +1 (positive correlation) to -1 (negative correlation), and a value of zero indicates no correlation (82). The value of r determines the strength of the association such that a value of r between 0.1-0.3 means there is a small association, 0.3-0.5 is medium, and 0.5-

1.0 indicates a large association between the two sets of variables. Since the computational scores are reported as positive values, we were looking for negative correlation coefficients; that is, as the value of the computational score increases, the value of the MIC decreases (Tables 5 and 6). Based on the correlation values, macromolecular targets with the highest negative correlation coefficients were deemed putative targets for our compounds.

Tables 5 and 6 represent the overall matrix of Pearson correlation coefficients based on all nine used scoring functions. Since the chemical structures of the two designed sets of compounds are different, their binding interactions with their putative targets are expected to be different; hence, their scores are expected to vary as well. The correlation coefficients for compounds **3a-3e** are shown in Table 5. The highest correlation coefficient between MIC values and calculated scores was obtained with LigScore-1 (LS1) when the compounds were docked into the acyl channel of KasA enzyme that showed a very high correlation value ($r = -0.99$). This high negative correlation means active compounds with low MIC values correlate with high docking scores. Moreover, for the same enzyme (KasA), another four scoring functions have got the highest correlation values with compounds **3a-3e** compared to other enzymes, namely PLP-1, PLP-2, Jain, and CDIE. Accordingly, compounds **3a-3e** are predicted to be most likely targeting the KasA enzyme. Yet, an *in vitro* enzyme assay will remain the main conclusive and decisive method to prove that compounds **3a-3e** have favorable binding affinity to mycobacterial KasA enzyme.

Table 5: The overall correlation coefficients matrix between the MIC values of compounds (**3a-3e**) and their computational scores obtained from different scoring functions for each of the selected target enzymes.

Index	Target	LS1	LS2	-PLP1	-PLP2	Jain	-PMF	-PMF04	-CDE	-CDIE
1	CamA	0.268	0.252	-0.084	0.205	-0.253	-0.248	0.68	-0.644	0.472
2	DprE1	0.559	0.201	0.937	0.307	0.34	-0.794	0.847	-0.58	0.828
3	FabH	-0.042	-0.256	0.035	-0.506	-0.459	0.35	0.553	-0.596	0.257
4	InhA	0.53	0.017	0.169	0.485	0.849	-0.909	-0.28	-0.342	0.567
5	MabA	0.655	0.72	0.729	0.743	0.621	0.473	0.76	-0.346	0.797
6	AspS	-0.066	-0.22	0.784	0.061	0.671	0.869	0.825	-0.811	-0.265
7	LeuRS	0.895	0.883	0.261	0.085	0.423	-0.236	0.666	-0.689	0.332
8	GlmU	0.288	0.218	0.141	-0.211	-0.66	0.821	0.691	-0.446	-0.031
9	PanK	0.227	0.04	0.048	-0.041	-0.147	0.172	0.403	-0.789	0.188
10	PknB	-0.401	-0.381	0.609	0.561	0.384	-0.207	0.286	-0.569	0.877
11	PknA	-0.566	-0.752	0.499	-0.024	-0.196	-0.461	0.846	0.005	0.641
12	KasA (BS-1)	-0.99	-0.741	-0.796	-0.911	-0.719	0.501	0.929	-0.616	-0.57
13	KasA (BS-2)*	0.965	0.721	0.926	0.994	0.686	0.888	0.965	0.313	0.996

14	Pks13	0.58	0.684	0.399	0.154	0.187	0.407	0.548	-0.713	0.817
15	BioA	0.849	-0.1	-0.254	0.043	0.537	0.788	0.997	-0.466	0.591
16	AspAT	0.419	0.043	0.362	-0.129	0.841	0.894	0.825	-0.802	-0.001
17	EchA6	0.811	0.957	0.953	0.824	0.88	0.929	0.923	-0.472	0.748
18	MurE	0.757	0.681	0.202	0.44	0.951	0.739	0.965	0.605	0.74
19	EthR	0.453	-0.6	-0.011	-0.282	0.488	0.989	0.791	-0.825	0.218
20	PrpC	0.824	0.911	0.736	0.289	0.969	0.439	0.623	-0.241	0.57

The highlighted values, in bold, represent the highest correlation coefficient scores for each scoring function.

*KasA has two binding sites, an acyl chain binding site (BS-1), and the catalytic active site (BS-2). Both were used for docking.

For the second set of compounds (**5a-5j**), the highest correlation was obtained using the PLP-2 scoring function when the compounds were docked into the active site of the BioA enzyme, as shown in Table 6. Accordingly, compounds **5a-5j** are predicted to be most likely targeting the BioA enzyme. Again, further investigation is needed to reach a decisive conclusion. Other important points that were considered when analyzing these results were; firstly, the two identified putative targets for compounds **3a-3e** and **5a-5j** had shown a general trend of having high negative correlation values with respect to various scoring functions compared to other enzymes. Secondly, the individual scores of the designed compounds showed higher or comparable values compared to the redocked native co-crystallized ligands. Particularly, the relative docking scores (RD) (83) of the most active compounds in the two sets (compounds **3d** and **5h**, respectively) were generally greater than 1, indicating that these compounds are expected to show good inhibitory potential against their respective targets (Tables 7 and 8). A comprehensive table of all docking scores and correlation values is available in supplementary materials (Table S1).

Table 6: The overall correlation matrix between the MIC values of compounds **5a-5j** and their computational scores obtained from different scoring functions for each of the selected enzymes.

Index	Name	LS1	LS2	-PLP1	-PLP2	Jain	-PMF	-PMF04	-CDE	-CDIE
1	CamA	-0.121	-0.435	-0.449	-0.289	0.141	-0.319	0	-0.348	-0.485
2	DprE1	0.146	0.114	-0.008	0.106	-0.484	-0.222	0.409	-0.231	0.096
3	FabH	0.131	0.185	0.291	-0.224	0.369	0.299	0.294	-0.141	0.187
4	InhA	0.773	0.663	0.33	0.663	0.169	0.348	0.528	-0.214	0.461
5	MabA	-0.109	-0.08	-0.147	-0.189	0.168	0.337	0.556	-0.216	-0.095
6	LeuRS	0.423	0.415	-0.27	-0.25	-0.164	-0.036	0.162	-0.109	0.003
7	GlmU	0.237	0.464	0.371	0.2	-0.103	0.665	0.719	-0.207	0.229
8	PanK	0.684	0.419	0.029	0.076	0.195	0.314	0.36	-0.296	0.015
9	PknB	0.184	-0.091	-0.55	-0.632	-0.316	-0.456	-0.017	-0.292	-0.088

10	PknA	0.808	0.479	0.199	-0.009	0.089	0.103	0.289	-0.2	0.219
11	KasA (BS-1)	0.068	-0.027	-0.591	-0.612	-0.291	0.194	0.3	-0.153	0.236
12	KasA (BS-2)*	0.717	0.326	0.666	0.658	0.60	0.46	0.530	-0.315	-0.082
13	Pks13	0.671	0.693	0.056	-0.243	-0.249	0.731	0.609	-0.385	-0.031
14	BioA	0.019	-0.261	-0.666	-0.715	-0.348	0.155	0.48	-0.289	-0.161
15	AspAT	0.296	0.384	0.601	0.454	-0.401	-0.613	-0.103	-0.15	0.37
16	EchA6	0.012	-0.132	-0.092	-0.178	0.03	-0.037	0.206	-0.178	0.295
17	MurE	0.608	0.568	0.226	0.271	-0.036	0.335	0.413	-0.131	0.433
18	EthR	-0.328	-0.256	-0.323	-0.384	0.22	-0.018	0.015	-0.145	-0.214
19	PrpC	-0.077	-0.16	-0.178	-0.069	-0.008	-0.024	0.031	-0.226	-0.314

The highlighted values, bold, represent the highest correlation coefficient scores for each scoring function.

*KasA has two binding sites, an acyl chain binding site (BS-1), and the catalytic active site (BS-2). Both were used for docking.

Table 7: The different scores of compounds **3a-3e** along with the relative docking score of compound **3d**.

Compounds' code	Scores									MIC ($\mu\text{g/mL}$)	
	LS1	LS2	-PLP1	-PLP2	Jain	-PMF	-PMF04	-CDE	-CDIE	HRv	MDR
3a	3.16	4.61	74.58	71.67	4.15	50.15	27.13	30.45	39.81	32	64
3b	3.20	5.06	86.72	81.18	4.77	53.28	29.83	33.14	43.01	32	64
3c	3.11	4.73	89.2	79.36	4.05	56.71	29.93	31.91	42.45	32	128
3d	3.58	5.07	94.14	85.10	3.72	51.79	26.92	27.47	40.14	16	128
3e	2.55	4.52	72.02	63.27	2.34	55.60	34.70	22.61	37.69	64	64
Co-crystallized ligand	3.34	5.27	78.04	69.82	3.93	38.43	20.73	22.21	42.06		
RD score of 3d*	1.07	0.96	1.21	1.22	0.95	1.35	1.30	1.24	0.95		

*RD score = compound's score/redocked co-crystallized ligand score

Table 8: The different scores of compounds **5a-5j** along with the relative docking score of compound **5h**.

Compounds' code	Scores									MIC ($\mu\text{g/mL}$)	
	LS1	LS2	-PLP1	-PLP2	Jain	-PMF	-PMF04	-CDE	-CDIE	HRv	MDR
5a	3.87	6.41	105.1	94.6	2.14	115.42	73.37	29.30	43.84	8	16
5b	4.16	5.96	87.77	83.32	1.9	114.57	85.38	30.52	43.04	10	20
5c	5.25	6.78	107.47	101.26	3.51	111.61	65.81	34.02	49.02	8	16
5d	5.23	6.55	91.53	78.41	1.5	127.86	96.17	27.222	46.25	16	64
5e	4.55	6.58	107.04	105.92	2.11	125.77	85.08	27.16	44.86	6	64
5f	4.63	6.47	98.91	94.62	2.39	126.04	87.92	28.17	45.57	11	32
5g	5.21	7.3	112.18	108.53	3.93	143.96	92.82	19.24	51.8	12	32
5h	5.36	6.98	114.1	108.7	3.95	129.98	95.25	16.73	47.79	5	16
5i	6.53	7.5	117.3	113.74	6.73	142.64	84.3	18.09	53.32	8	16

5j	5.06	6.35	91.9	83.81	2.55	128.16	96.46	7.53	44.15	16	16
Co-crystallized ligand	3.47	6.4	110.98	108.81	4.35	89.27	59.98	5.26	47.54	--	--
RD score of 5h*	1.55	1.09	1.03	1.0	0.91	1.46	1.59	3.18	1.01	--	--

*RD score = compound's score/redocked co-crystallized ligand score

3.4.2 Analysis of the Binding Interactions of the most Active Compounds with their Putative Targets

In this study, the mycobacterial β -ketoacyl acyl carrier protein synthase I (KasA) enzyme has been identified as a putative target for compounds **3a-3e**. Biologically, this enzyme catalyzes the condensation reaction of fatty acid synthesis by the addition of two carbons from malonyl-ACP to the growing acyl chain in mycolic acid synthesis (84). Mycolic acids, long α -alkyl- β -hydroxy fatty acids comprising 60–90 carbon atoms, are essential components of the mycobacterial cell wall and are also critical for mycobacterial persistence and pathogenesis (85). An interplay of two distinct fatty acid biosynthesis pathways is required for the biosynthesis of mycolic acids, namely the mammalian-like type I (FAS-I) and the bacterial type II (FAS-II) systems. The FAS-I primer products are elongated by the FAS-II pathway to produce mycolic acid precursors (termed meromycolates). Contrary to the FAS-I system, which is composed of one large multifunctional dimer, the FAS-II system is composed of monofunctional enzymes. The KasA enzyme is a key player in the FAS-II system; therefore, inhibitors of this important enzyme represent potential antimycobacterial agents (86).

Structurally, the KasA enzyme is composed of a core domain and a cap (Figure 6). The core domain is divided into two topologically similar halves and is hosting the residues of the catalytic triad, Cys171, His311, and His345. A large acyl channel that normally accommodates the growing meromycolic acid chain constitutes the entrance to the catalytic binding site (Figure 6). Different inhibitors have been identified that target the catalytic active site of KasA enzyme (86); however, the acyl channel has been the focus of many recent drug discovery efforts aiming to develop clinically useful anti-tubercular agents. The latter approach offers an opportunity to achieve the desired selectivity over other related β -ketoacyl synthases, such as FabH and KasB, that are involved in fatty acid biosynthesis due to the non-conservation of key binding residues in other enzymes (87).

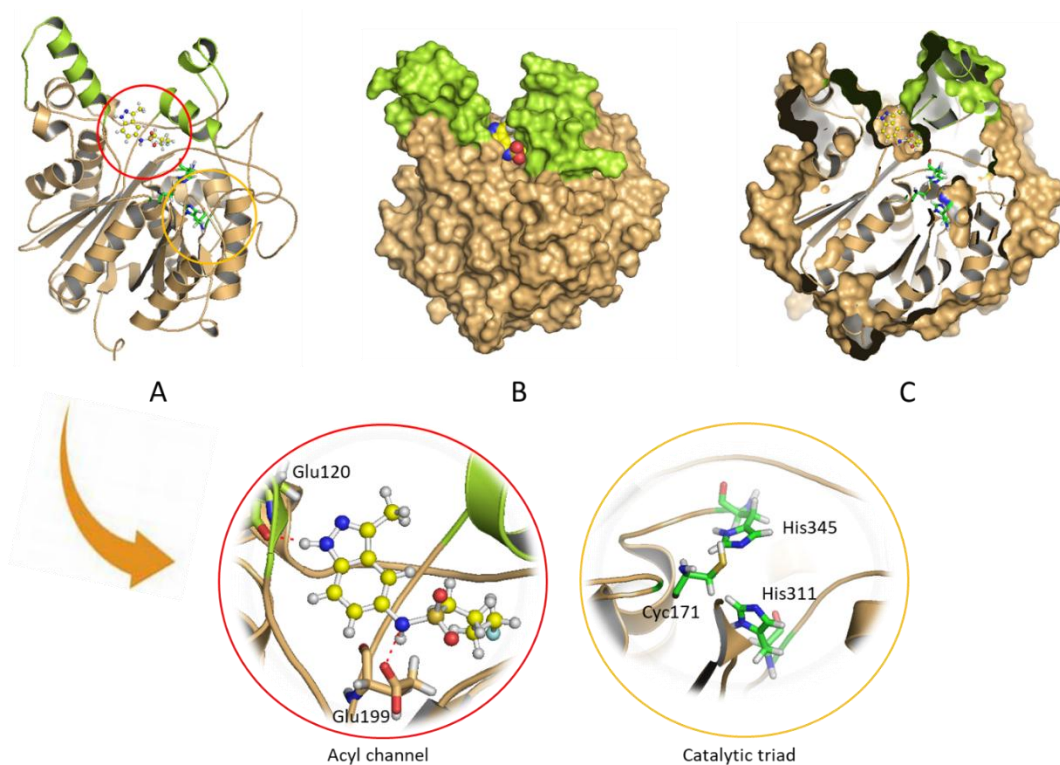


Figure 6: The 3D crystal structure of the *Mycobacterium tuberculosis* KasA enzyme (PDB code 6P9L). A. Cartoon representation of the enzyme. The core domain is colored light orange, and the cap is green. The co-crystallized inhibitor is represented in balls and sticks with carbons colored yellow. The catalytic triad is shown in the sticks with their carbons colored green. The acyl channel and the catalytic triad are highlighted with red and yellow circles, and a close-up view of them is shown underneath. B. Solvent-accessible surface representation of the enzyme with the co-crystallized inhibitor is shown in CPK. C. A clipped view of (B) shows the position of the acyl channel relative to the catalytic triad.

In this study, two different docking experiments have been conducted in order to investigate the binding affinity of the tested compounds towards the two distinct KasA binding sites, the catalytic active site and the acyl channel. The structural models of the KasA enzyme were obtained from the protein data bank with accession codes of 6P9L, which corresponds to the MTB KasA enzyme in complex with a potent pre-clinical inhibitor (JSF-3285) binding the acyl channel at a resolution of 2.31 Å; and 2WGE, which corresponds to mycobacterial KasA enzyme in complex with the antibiotic thiolactomycin binding the catalytic active site at a resolution of 1.80 Å (88). Then, they were prepared as detailed in the methods section. Prior to docking the designed compounds into KasA binding sites, the docking protocol was validated by redocking the co-crystallized inhibitors into their respective binding sites, which showed perfect alignment with the native co-crystallized poses with RMSD of 0.550 Å and 0.197 Å for 6P9L (acyl channel) and 2WGE (catalytic active site), respectively (Figure S1). The docking results revealed that our compounds have a preferential binding affinity towards the acyl channel, which was reflected by higher docking scores. Figure 7 shows the binding

orientation and binding interactions of compound **3d** within the acyl channel of the KasA enzyme compared to that of the preclinical candidate co-crystallized ligand (JSF-3285).

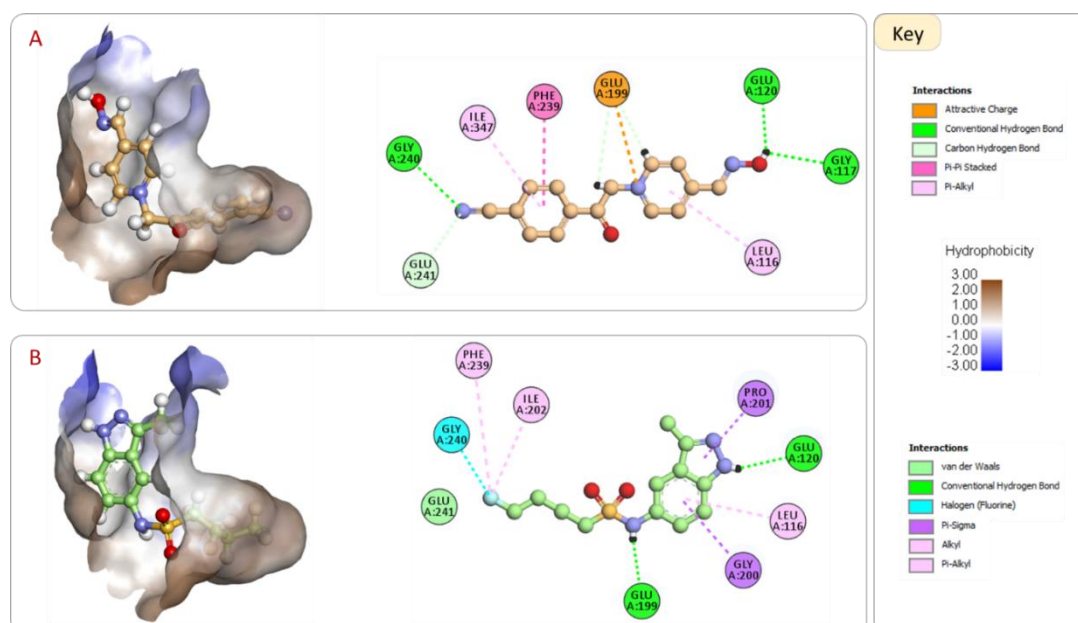


Figure 7: The binding orientation and binding interactions of compound **3d** within the acyl channel of the KasA enzyme (A) compared to that of the co-crystallized ligand (JSF-3285, PDB code 6P9L) (B). The left panel shows the binding orientations of compound **3d** and JSF-3285. The acyl channel is shown as a hydrophobic surface. The right panel shows the 2D interaction maps of the two compounds. The interacting amino acid residues are represented as disks colored according to the type of interactions they are forming with the enzyme.

As shown in Figure 7, the cyanophenyl moiety of compound **3d** is inserted into a hydrophobic pocket and forms hydrophobic interactions with Phe239 and Ile347 and a hydrogen bond with Gly240, overall mimicking the aliphatic moiety of JSF-3285, which in turn mimics the binding of the phospholipid acyl tail. Moreover, compound **3d** is establishing further stabilizing interactions, including electrostatic interaction between the pyridinium nitrogen and the important Glu199, hydrogen bonding between the oxime oxygen and the important Glu120, and another hydrogen bond with Gly117, a hydrophobic interaction between the pyridinium ring and Leu116. Based on these interactions, compound **3d** is expected to have a favorable binding affinity towards the KasA enzyme that could be experimentally assessed via *in vitro* enzyme assay.

For compounds **5a-5j**, the mycobacterial PLP-dependent aminotransferase (BioA) enzyme has been identified as a putative target. This enzyme catalyzes the second step in biotin biosynthesis and is essential for bacterial survival and persistence. Contrary to humans, MTB *de novo* synthesizes biotin to be utilized by carboxylases in fatty acid metabolism and gluconeogenesis pathways; thereby, BioA is an ideal target for the development of potential anti-tubercular agents (70).

Structurally, the functional form of the mycobacterial BioA enzyme is a homodimer, in which the monomer structure is composed of two domains, the small domain (amino acid residues 1-60 and 339-437) and the large domain (residues 61-338). Two active sites are located at the interface between the two monomers, 18 Å apart, and are composed of residues Pro24-Ser34, Ser62-Ala67, Arg156-Asp160, His171-Arg181, Gln224-Gly228, and Arg400-Arg403 from one chain, and Met'87-His'97 and Ala'307-Asn'322 from the other chain (70, 89, 90). Among these residues, Tyr25, Trp64, Trp65, Tyr157, Arg400, and Phe402 were reported to be of high relevance to ligand binding (90, 91) (Figure 8).

The structural model of the MTB BioA enzyme was obtained from the protein data bank (PDB code, 4XJO), which corresponds to the BioA enzyme in complex with an inhibitor, 5-[4-(3-chlorobenzoyl)piperazin-1-yl]-1*H*-inden-1-one (410), and the coenzyme PLP at a resolution of 1.50 Å, then it was prepared as detailed in the methods section. The docking protocol was validated, before docking the designed compounds, via redocking the co-crystallized ligand (410). The redocked pose was in excellent agreement with the native co-crystallized ligand pose with an RMSD of 0.15 Å. Then, the designed compounds were docked into the active site of the enzyme. Figure 9 shows the binding orientation and binding interactions of compound 5h within the active site of the KasA enzyme compared to that of the co-crystallized ligand (410).

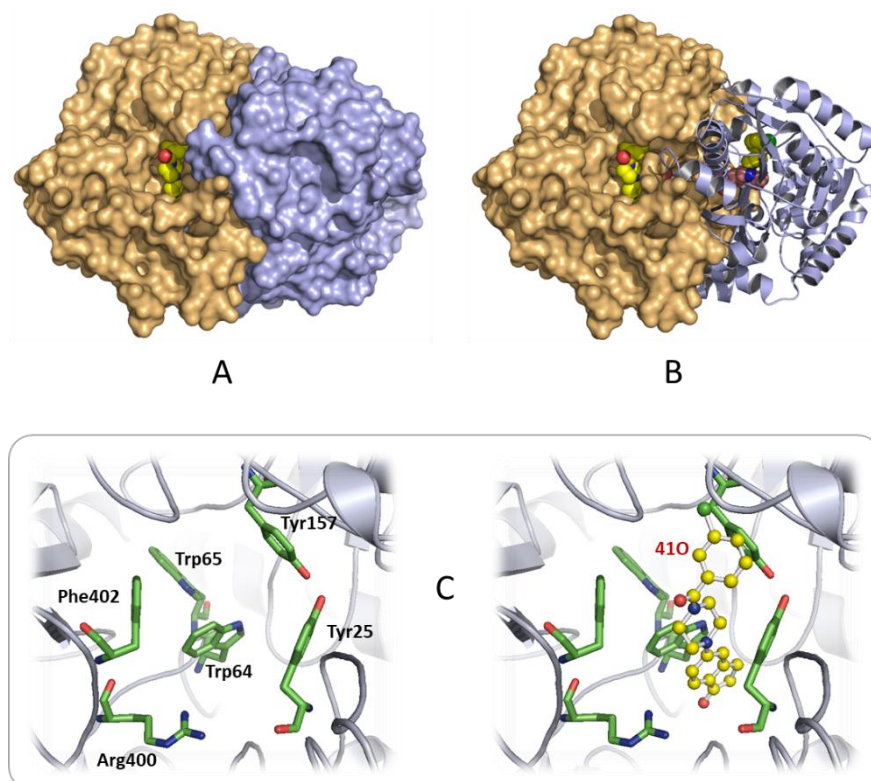


Figure 8: The 3D crystal structure of the mycobacterial BioA enzyme (PDB code 4XJO). A. The homodimer enzyme is shown as a surface with monomers colored differently. The co-crystallized

inhibitors are shown in CPK representation with carbons colored yellow. B. Same view as in A, where monomer B is shown in a cartoon to highlight the location of the two active sites. The PLP molecule is shown in CPK representation with carbons colored pink. C. Close-up views of the active site with and without the co-crystallized ligand highlight the main binding residues that are depicted as sticks with carbons colored green.

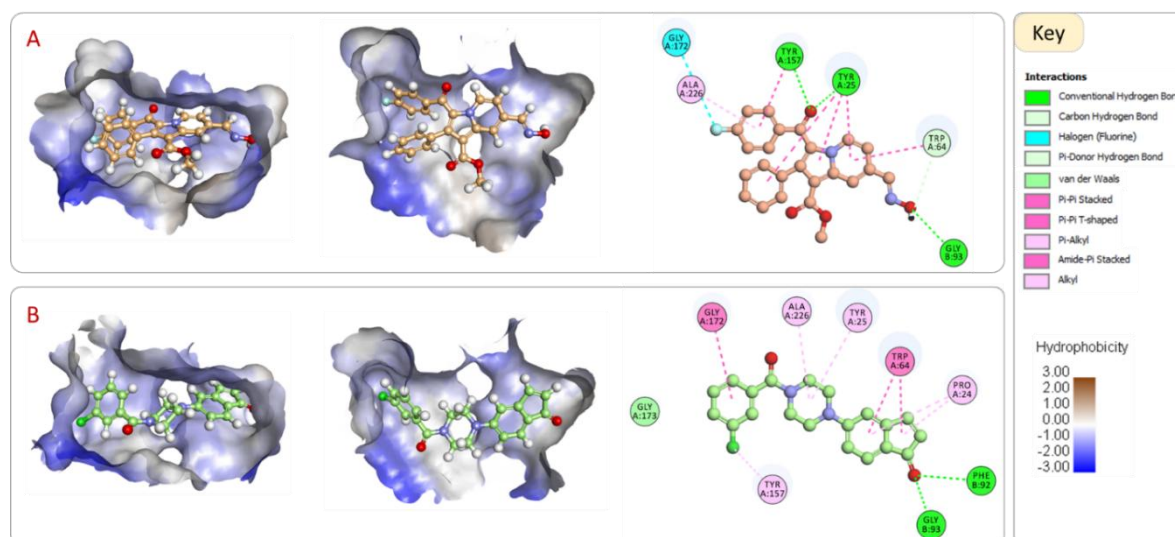


Figure 9: A. The binding orientation and binding interactions of compound **5h** within the active site of the BioA enzyme compared to that of the co-crystallized ligand (410, PDB code 4XJO) in (B). The left panel shows the binding orientations of compounds **5h** and 410. The active site is shown as a hydrophobic surface. The right panel shows the 2D interaction maps of the two compounds. The interacting amino acid residues are represented as disks colored according to the type of interactions they are forming with the enzyme.

As shown in Figure 9, compound **5h** fully occupies the binding pocket of the active site and the 2D interaction map shows the involvement of many key binding residues within the active site. Compound **5h** establishes three hydrogen bonds with the amino acid residues Tyr25, Gly93, and Tyr157. Also, it exhibited numerous hydrophobic interactions, including π - π stacking with Tyr25, Trp64, Tyr157, π - π T-shaped with Tyr25, π -alkyl with Ala226, and a halogen bond with Gly172. Again, based on these interactions, compound **5h** seems to have a favorable binding affinity towards the BioA enzyme that could be experimentally assessed via *in vitro* enzyme assay.

Once the mechanism of action of compounds **3d** and **5h** have been confirmed as being, respectively, mycobacterial KasA and BioA inhibitors, their detailed binding interactions can be utilized to guide prospective optimization of these lead compounds towards designing more potent and selective drug candidates.

3.4.3 The Docking Results of Compounds 3d and 5h against InhA Enzyme

Since the two sets of compounds were *in vitro* tested against the InhA enzyme, though they showed poor correlation with their MIC values, which agrees with the above docking results, their docking results against the InhA enzyme are briefly discussed below in light with their results against KasA and BioA enzymes.

Table 9 shows the docking scores and the RD scores of the tested compounds against the InhA enzyme. It is obvious that the docking scores are generally lower than their corresponding scores against the KasA (for compounds **3a-e**, Table 7) and BioA (for compounds **5a-j**, Table 8), which are reflected by having lower RD scores. Moreover, Table 9 shows higher docking scores for compounds **5a-j** against the InhA enzyme compared to compounds **3a-e**, which agrees with the *in vitro* testing results in which compounds **5a-j** showed better inhibitory activities against the InhA enzyme. The agreement between the computational and the experimental results suggests that the computationally identified putative targets are highly likely to be the actual targets for our compounds. Yet, further *in vitro* testing is needed to confirm this conclusion.

Table 9: The different docking scores of compounds **3a-e** and **5a-5j** against the InhA enzyme along with relative docking scores of compounds **3a**, **5h**, and **5f**.

Compounds' code	Scores									MIC ($\mu\text{g/mL}$)	
	LS1	LS2	PLP1	PLP2	Jain	PMF	PMF4	CDE	CDIE	HRv	MDR
3a	3.16	5.13	74.66	71.91	3.13	77.39	41.77	27.29	37.38	32	64
3b	3.51	5.43	80.59	72.53	3.06	76.67	40.45	31.76	39.88	32	64
3c	3.82	5.01	72.43	65.11	3.36	72.84	33.54	26.40	35.68	32	128
3d	3.49	5.27	79.94	71.37	2.55	76.82	28.81	27.43	37.92	16	128
3e	3.86	5.25	80.13	75.28	3.53	63.45	27.65	25.83	40.53	64	64
5a	4.17	6.1	96.9	91.76	3.67	112.4	36.58	30.92	44.89	8	16
5b	3.78	5.95	97.43	89.88	4.17	108.72	40.29	30.32	45.73	10	20
5c	4.16	6.12	100.2	93.1	4.21	111.86	32.44	31.12	44.57	8	16
5d	4.79	6.23	96.41	91.02	3.06	121.25	59.84	28.91	47.22	16	64
5e	4.2	6.2	88.12	84.53	3.31	120.23	43.73	30.15	50.16	6	64
5f	4.41	6.39	95.96	93.81	3.36	128.93	53.32	27.64	46.28	11	32
5g	3.89	6	100.65	90.92	4.61	114.81	29.94	9.96	50.05	12	32
5h	3.31	5.71	98.71	83.74	3.33	114.9	31.29	8.93	44.28	5	16
5i	4.12	6.02	107.76	95.58	5.02	138.52	36.97	8.96	47.13	8	16
5j	5.64	6.62	107.38	106.54	4.8	136.76	40.88	-0.58	50.59	16	16
Co-crystallized ligand	3.83	5.55	86.45	88.49	5.12	90.07	35.03	12.81	41.31		
RD* score of 3a	0.91	0.95	0.92	0.81	0.50	0.85	0.82	2.14	0.92		
RD score of 5d	0.86	1.03	1.14	0.95	0.65	1.28	0.89	0.70	1.07		
RD score of 5f	1.15	1.15	1.11	1.06	0.66	1.43	1.52	2.16	1.12		

*RD score = compound's score/redocked co-crystallized ligand score

3.5 ADMET Predictions

In any drug discovery process, it is empirical to focus lead optimization efforts on lead compounds with favorable ADMET properties to avoid dead ends due to unfavorable ADMET characteristics. The biological results of our tested compounds were quite encouraging and worthy of further optimization. Therefore, their ADMET parameters were calculated to aid prospective optimization and to focus on lead compounds with favorable ADMET properties.

Various ADMET descriptors, including aqueous solubility (AS), blood-brain barrier (BBB) penetration, CYP2D6 inhibition, hepatotoxicity, human intestinal absorption (HIA), plasma protein binding (PPB), AlogP, and polar surface area (PSA) were calculated using the ADMET Descriptors protocol in DS (Table 10). Likewise, different toxicity parameters were also calculated using the Toxicity Prediction (TOPKAT) protocol including rodent carcinogenicity (for male and female rats and mice, CMR, CFR, and CLM, CFM respectively), Ames mutagenicity (AM), skin irritation (SI), ocular irritancy (OI), aerobic biodegradability and developmental toxicity potential (AB) (Table 10). Based on the results presented in Table 10, the tested compounds show promising ADMET profiles. Hence, the most active ones could be considered leads worthy of further optimization.

Table 10: Calculated ADMET descriptors and toxicity parameters

Code	MIC (µg/mL)		ADMET descriptors ^a									Toxicity parameters ^b							
	H37 Rv	MD R-MTB	A S	BB B	CYP2D6 inhibition	Hepatotoxicity	HI A	PPB	AlogP	PSA	AM	SI	OI	AB	DTP	CMR	CFR	CLM	CFM
3a	32	64	3	2	FALSE	TRUE	0	FALSE	1.88	54.78	0.001	1	0	0	0.066	0.917	0.001	0.996	1
3b	32	64	3	2	FALSE	TRUE	0	FALSE	2.63	54.78	0	0.991	0	0	0.058	0.885	0	1	1
3c	32	128	3	2	FALSE	TRUE	0	TRUE	2.08	54.78	0	1	0	0	0.058	0.885	0	1	1
3d	16	128	3	3	FALSE	TRUE	0	FALSE	1.76	77.72	0.31	0.834	0	0	0.061	0.917	0	0.059	1
3e	64	64	3	3	FALSE	TRUE	0	FALSE	1.77	97.61	0.361	0.123	0.151	0	0.023	0.958	0.983	0.004	1
5a	8	16	2	2	FALSE	FALSE	0	TRUE	3.40	81.01	0	0.001	0	0	0.023	0.500	0	0.058	1
5b	10	20	2	2	FALSE	TRUE	0	TRUE	3.61	81.01	0	0.096	0	0	0.015	0.700	0	0.996	1
5c	8	16	2	4	FALSE	TRUE	0	TRUE	3.28	103.9	0.005	0	0	0	0.001	0.700	0	0	1
5d	16	64	2	4	FALSE	TRUE	1	TRUE	3.30	123.8	0.045	0	0	0	0.055	0.900	0.005	0	1
5e	6	64	2	2	FALSE	TRUE	0	TRUE	4.64	81.01	0	0.001	0	0	0.061	0.729	0	0	1
5f	11	32	2	2	FALSE	TRUE	0	TRUE	4.1	81.01	0	0.045	0	0	0.084	0.729	0	0.071	1
5g	12	32	1	4	FALSE	TRUE	1	TRUE	5.32	81.01	0	0.001	0	0	0.084	0.900	0	0	1
5h	5	16	2	1	FALSE	TRUE	0	TRUE	4.78	81.01	0	0.079	0	0	0.084	0.900	0	0.008	1
5i	8	16	2	4	FALSE	TRUE	1	TRUE	4.45	103.9	0	0	0	0	0.084	0.900	0	0	1
5j	16	16	2	4	FALSE	TRUE	2	TRUE	4.47	123.8	0	0.001	0	0	0.099	0.999	0.029	0	1

^a Key to the above calculated ADMET descriptors

Aqueous Solubility (AS)			Blood-Brain Barrier (BBB) Penetration			Human Intestinal Absorption (HIA)		
Level	Value	Drug-likeness	Level	Value	Description	Level	Description	
0	$\log(Sw) < -8.0$	Extremely low	0	Very High	Brain-Blood ratio greater than 5:1	0	Good absorption	
1	$-8.0 < \log(Sw) < -6.0$	No, very low, but possible	1	High	Brain-Blood ratio between 1:1 and 5:1	1	Moderate absorption	
2	$-6.0 < \log(Sw) < -4.1$	Yes, low	2	Medium	Brain-Blood ratio between 0.3:1 and 1:1	2	Low absorption	
3	$-4.1 < \log(Sw) < -2.0$	Yes, good	3	Low	Brain-Blood ratio less than 0.3:1	3	Very low absorption	
4	$-2.0 < \log(Sw) \leq 0.0$	Yes, optimal	4	Undefined	Outside 99% confidence ellipse			
5	$0.0 < \log(Sw)$	No, too soluble						

^b Key to the above calculated toxicity parameters

Probability values	Probability level	Description
0.0 to 0.30	Low probability	Such a chemical is not likely to produce a positive response in an experimental assay
Greater than 0.30 but less than 0.70	Intermediate probability	
Greater than 0.70	High probability	Likely to produce a positive response in an experimental assay

4. Conclusion

In the present study, the anti-tubercular activity of two sets of compounds, **3a-3e** and **5a-5j**, were biologically evaluated against two strains of MTB, namely H37Rv, and MDR. The *in vitro* results showed excellent inhibitory activities against both MTB strains. Compounds **5a-5j** were found to be more potent than **3a-3e**, with MIC values ranging from 5-16 $\mu\text{g}/\text{mL}$ and 16-64 $\mu\text{g}/\text{mL}$ against H37Rv and MDR, respectively, of which compound **5h** was the most active with a MIC of 5 $\mu\text{g}/\text{mL}$ and 16 $\mu\text{g}/\text{mL}$ against H37Rv and MDR-TB strains, respectively.

Further, all compounds were also tested *in vitro* against the mycobacterial InhA enzyme. However, the compounds **3a-3e** and **5a-5h** showed weak to moderate activities against the InhA enzyme that ranged from 5-17% and 10-52% inhibition, respectively, with compound **5f** containing methyl and 4-fluorobenzoyl groups attached to the 2- and 3-positions of the indolizine core being the most active (52% inhibition of InhA). It is interesting to note that the presence of substituent at the 2-position of the indolizine scaffold increased the activity for 4-fluorobenzoyl containing compounds **5f** and **5h** as compared to the compound **5b** with unsubstituted 2-position of the scaffold. However, compound **5f** with a methyl group at the 2-position of indolizine was found to be the most active (52% inhibition of InhA) as compared to the compound **5h** containing a bulky phenyl group at the same position (35% inhibition of InhA).

However, the MIC values were not correlated with the InhA *in vitro* inhibition assay results, which suggests that different mechanism(s) of action for these compounds, other than InhA inhibition, are highly likely. Therefore, a computational approach was employed in order to identify their putative target(s), which ultimately would explain their mechanism of action.

The computational results revealed the KasA and BioA enzymes as the putative targets for compounds **3a-3e** and **5a-5j**, respectively. Moreover, *in silico* ADMET predictions showed adequate properties for these compounds, making them promising leads worthy of further optimization.

Acknowledgements

The authors extend their appreciation to the Deputyship for Research & Innovation, Ministry of Education in Saudi Arabia for funding this research work through the project number 1058, King Faisal University, Kingdom of Saudi Arabia for support and encouragement, the Department of Microbiology, National Health Laboratory Services, Inkosi Albert Luthuli Central Hospital, Durban South Africa for providing the facility to carry out *in vitro* anti-TB activity, and Dr. Hong Su, Center for Supramolecular Chemistry Research, Department of Chemistry, University of Cape Town, South

Africa, for single-crystal X-ray data collection. The authors are thankful to the Faculty of Pharmacy, Philadelphia University, Jordan, and the Faculty of Pharmacy, Jordan University of Science and Technology, Irbid, Jordan, for providing the necessary laboratory facilities to carry out this research project. P.K.D thanks BIT Mesra, Ranchi for its research facilities and infrastructure. D.C. thanks IISER Bhopal for its research facilities and infrastructure. S.C. thanks NIPER Raebareli for its research facilities and infrastructure. The authors wish to thank Mr. Tameem M. Alyahian for providing technical support in this project. R.T., C.L and L.M. are indebted to the Université fédérale Toulouse Midi-Pyrénées and the Région Occitanie for their support (PhD grant to R.T.).

Disclosure statement

Authors declare that they have no competing interest.

Funding

This research was funded by the Deputyship for Research & Innovation, Ministry of Education in Saudi Arabia (Research Project Number 1058).

References

1. Barberis I, Bragazzi NL, Galluzzo L, & Martini M (2017) The history of tuberculosis: from the first historical records to the isolation of Koch's bacillus. *J Prev Med Hyg* 58(1):E9-E12.
2. Gradmann C (2001) Robert Koch and the pressures of scientific research: tuberculosis and tuberculin. *Med Hist* 45(1):1-32.
3. Kompala T, Shenoj SV, & Friedland G (2013) Transmission of tuberculosis in resource-limited settings. *Curr HIV/AIDS Rep* 10(3):264-272.
4. Lee JY (2015) Diagnosis and treatment of extrapulmonary tuberculosis. *Tuberc Respir Dis (Seoul)* 78(2):47-55.
5. Pai M, *et al.* (2016) Tuberculosis. *Nat Rev Dis Primers* 2:16076.
6. Anonymous (World Health Organization. Global tuberculosis report 2019 (Executive summary). https://www.who.int/tb/publications/global_report/tb19_Exec_Sum_12Nov2019.pdf?ua=1 (accessed September 9, 2020).
7. World Health Organization (2020) Global tuberculosis report 2020. (Geneva).
8. Silva DR, *et al.* (2018) Risk factors for tuberculosis: diabetes, smoking, alcohol use, and the use of other drugs. *J Bras Pneumol* 44(2):145-152.
9. Anonymous (World Health Organization. Guidelines for treatment of drug-susceptible tuberculosis and patient care: 2017 update. <https://apps.who.int/iris/handle/10665/255052> (visited on August 29, 2021).
10. Tetali SR, *et al.* (2020) Current advances in the clinical development of anti-tubercular agents. *Tuberculosis* 125:101989.
11. Anonymous (World Health Organization. WHO consolidated guidelines on drug-resistant tuberculosis treatment 2019 file:///C:/Users/VenuG/Downloads/9789241550529-eng.pdf (visited on August 29, 2021).

12. Borah P, *et al.* (2021) Tuberculosis: An update on pathophysiology, molecular mechanisms of drug resistance, newer anti-tb drugs, treatment regimens and host- directed therapies. *Curr. Top. Med. Chem.* 21(6):547-570.
13. Saxena AK & Singh A (2019) Mycobacterial tuberculosis Enzyme Targets and their Inhibitors. *Curr. Top. Med. Chem.* 19(5):337-355.
14. Li Y, Sun F, & Zhang W (2019) Bedaquiline and delamanid in the treatment of multidrug-resistant tuberculosis: Promising but challenging. *Drug Development Research* 80(1):98-105.
15. Anonymous (Food and Drug Administration. FDA approves new drug for treatment-resistant forms of tuberculosis that affects the lungs. FDA 2019. <https://www.fda.gov/news-events/press-announcements/fda-approves-new-drug-treatment-resistant-forms-tuberculosis-affects-lungs> (accessed October 5, 2020).
16. Bloemberg GV, *et al.* (2015) Acquired Resistance to Bedaquiline and Delamanid in Therapy for Tuberculosis. *N. Engl. J. Med.* 373(20):1986-1988.
17. Maeurer M, Schito M, & Zumla A (2014) Totally-drug-resistant tuberculosis: hype versus hope. *Lancet Respir Med* 2(4):256-257.
18. Alveera S, *et al.* (2017) Antimycobacterial, docking and molecular dynamic studies of pentacyclic triterpenes from *Buddleja saligna* leaves. *J. Biomol. Struct. Dyn.* 35(12):2654-2664.
19. Venugopala KN, *et al.* (2011) Total synthesis of a depsidomycin analogue by convergent solid-phase peptide synthesis and macrolactonization strategy for antitubercular activity. *Journal of Peptide Science* 17(10):683-689.
20. Venugopala KN, *et al.* (2020) Anti-tubercular properties of 4-amino-5-(4-fluoro-3-phenoxyphenyl)-4H-1,2,4-triazole-3-thiol and its schiff bases: computational input and molecular dynamics. *Antibiotics* 9(9):559.
21. Venugopala KN, *et al.* (2013) Synthesis and antitubercular activity of 2-(substituted phenyl/benzyl-amino)-6-(4-chlorophenyl)-5-(methoxycarbonyl)-4-methyl-3,6-dihydropyrimidin-1-ium chlorides. *Chem. Biol. Drug Des.* 81(2):219-227.
22. Venugopala KN, *et al.* (2020) In silico design and synthesis of tetrahydropyrimidinones and tetrahydropyrimidinethiones as potential thymidylate kinase inhibitors exerting anti-TB activity against *Mycobacterium tuberculosis*. *Drug Des. Devel. Ther.* 14:1027.
23. Venugopala KN, *et al.* (2016) Design, synthesis, and characterization of (1-(4-aryl)-1H-1,2,3-triazol-4-yl)methyl, substituted phenyl-6-methyl-2-oxo-1,2,3,4-tetrahydropyrimidine-5-carboxylates against *Mycobacterium tuberculosis*. *Drug Design, Development and Therapy* 10:2681-2690.
24. Venugopala KN, *et al.* (2019) Synthesis and structural elucidation of novel benzothiazole derivatives as anti-tubercular agents: In-silico screening for possible target identification. *Medicinal Chemistry* 15(3):311-326.
25. Venugopala KN, *et al.* (2019) Benzothiazole analogs as potential anti-TB agents: computational input and molecular dynamics. *Journal of Biomolecular Structure and Dynamics* 37(7):1830-1842.
26. Venugopala KN, *et al.* (2020) Cytotoxicity and antimycobacterial properties of pyrrolo[1,2-a]quinoline derivatives: Molecular target identification and molecular docking studies. *Antibiotics* 9(5):1-14.
27. Hasija A, Bhandary S, Venugopala KN, Chandrashekarappa S, & Chopra D (2020) Structural investigation of methyl 3-(4-fluoro-benzo-yl)-7-methyl-2-phenyl-indolizine-1-carboxyl-ate, an inhibitory drug towards *Mycobacterium tuberculosis*. *Acta Crystallogr E Crystallogr Commun* 76(Pt 4):567-571.
28. Venugopala KN, *et al.* (2019) Anti-tubercular activity of substituted 7-methyl and 7-formylindolizines and in silico study for prospective molecular target identification. *Antibiotics* 8(4).

29. Khedr MA, *et al.* (2018) Molecular modeling studies and anti-TB activity of trisubstituted indolizine analogues; molecular docking and dynamic inputs. *J. Biomol. Struct. Dyn.* 36(8):2163-2178.
30. Venugopala KN, *et al.* (2019) Anti-tubercular potency and computationally-assessed drug-likeness and toxicology of diversely substituted indolizines. *Indian Journal of Pharmaceutical Education and Research* 53(3):545-552.
31. Venugopala KN, *et al.* (2019) Computational, crystallographic studies, cytotoxicity and anti-tubercular activity of substituted 7-methoxy-indolizine analogues. *PLoS One* 14(6):e0217270.
32. Rai NP, *et al.* (2010) Design, synthesis, characterization, and antibacterial activity of {5-chloro-2-[(3-substitutedphenyl)-1,2,4-oxadiazol-5-yl]-methoxy}-phenyl-(phenyl)-methanones. *European Journal of Medicinal Chemistry* 45(6):2677-2682.
33. Venugopala KN (2017) Design, microwave assisted synthesis and characterization of substituted 1, 2, 4-oxadiazole analogues as promising pharmacological agents. *Asian Journal of Chemistry* 29(8):1767-1770.
34. Deb PK, Al-Shar'i NA, Venugopala KN, Pillay M, & Borah P (2021) In vitro anti-TB properties, in silico target validation, molecular docking and dynamics studies of substituted 1, 2, 4-oxadiazole analogues against *Mycobacterium tuberculosis*. *J. Enzyme Inhib. Med. Chem.* 36(1):869-884.
35. Venugopala KN, *et al.* (2021) Anti-tubercular activity and molecular docking studies of indolizine derivatives targeting mycobacterial InhA enzyme. *J. Enzyme Inhib. Med. Chem.* 36(1):1472-1487.
36. Venugopala KN & Sandeep C (2020) Novel substituted indolizine scaffolds for MDR strains of *Mycobacterium tuberculosis*, synthetic methodology and chemical structures thereof. *Indian Patent* IN201941002546A.
37. Rovnyak GC, *et al.* (1992) Dihydropyrimidine calcium channel blockers. 4. Basic 3-substituted-4-aryl-1,4-dihydropyrimidine-5-carboxylic acid esters. Potent antihypertensive agents. *J. Med. Chem.* 35(17):3254-3263.
38. Sheldrick GM (2008) A short history of SHELX. *Acta Crystallographica Section A* 64(Pt 1):112-122.
39. Sheldrick G (2015) SHELXT - Integrated space-group and crystal structure determination. *Acta Crystallographica Section A* 71:3-8.
40. Spek A (2020) checkCIF validation ALERTS: what they mean and how to respond. *Acta Crystallographica Section E* 76(1):1-11.
41. Farrugia L, J (2012) WinGX and ORTEP for Windows: an update. *Journal of Applied Crystallography* 45(4):849-854.
42. Macrae CF, *et al.* (2006) Mercury: visualization and analysis of crystal structures. *Journal of Applied Crystallography* 39(3):453-457.
43. Martin A, *et al.* (2005) Multicenter study of MTT and resazurin assays for testing susceptibility to first-line anti-tuberculosis drugs. *International Journal of Tuberculosis and Lung Disease* 9(8):901-906.
44. Middlebrook G, Reggiards Z, & Tigertt WD (1977) Automable radiometric detection of growth of *Mycobacterium tuberculosis* in selective media. *Am. Rev. Respir. Dis.* 115:1067-1069.
45. Doğan H, *et al.* (2020) Discovery of hydrazone containing thiadiazoles as *Mycobacterium tuberculosis* growth and enoyl acyl carrier protein reductase (InhA) inhibitors. *Eur. J. Med. Chem.* 188:112035.
46. Keleş Atıcı R, *et al.* (2022) Urea derivatives carrying a thiophenylthiazole moiety: Design, synthesis, and evaluation of antitubercular and InhA inhibitory activities. *Drug Development Research* 83(6):1292-1304.
47. DeLano WL (The PyMOL Molecular Graphics System (Schrödinger, LLC), 0.99rc6.

48. Menendez C, *et al.* (2012) Chemical synthesis and biological evaluation of triazole derivatives as inhibitors of InhA and antituberculosis agents. *Eur. J. Med. Chem.* 52:275-283.
49. Menendez C, *et al.* (2011) Synthesis and biological activities of triazole derivatives as inhibitors of InhA and antituberculosis agents. *Eur. J. Med. Chem.* 46(11):5524-5531.
50. Yuan T & Sampson NS (2018) Hit Generation in TB Drug Discovery: From Genome to Granuloma. *Chemical Reviews* 118(4):1887-1916.
51. Wang F, *et al.* (2013) Identification of a small molecule with activity against drug-resistant and persistent tuberculosis. *Proceedings of the National Academy of Sciences* 110(27):E2510-E2517.
52. Torfs E, Piller T, Cos P, & Cappoen D (2019) Opportunities for Overcoming Mycobacterium tuberculosis Drug Resistance: Emerging Mycobacterial Targets and Host-Directed Therapy. *International journal of molecular sciences* 20(12):2868.
53. Piton J, Foo CSY, & Cole ST (2017) Structural studies of Mycobacterium tuberculosis DprE1 interacting with its inhibitors. *Drug Discovery Today* 22(3):526-533.
54. Kamsri P, *et al.* (2020) Discovery of New and Potent InhA Inhibitors as Antituberculosis Agents: Structure-Based Virtual Screening Validated by Biological Assays and X-ray Crystallography. *Journal of Chemical Information and Modeling* 60(1):226-234.
55. Huang C-c, Smith CV, Glickman MS, Jacobs WR, & Sacchettini JC (2002) Crystal Structures of Mycolic Acid Cyclopropane Synthases from Mycobacterium tuberculosis. *Journal of Biological Chemistry* 277(13):11559-11569.
56. Shetye GS, Franzblau SG, & Cho S (2020) New tuberculosis drug targets, their inhibitors, and potential therapeutic impact. *Translational Research* 220:68-97.
57. Ioerger TR, *et al.* (2013) Identification of New Drug Targets and Resistance Mechanisms in Mycobacterium tuberculosis. *PLOS ONE* 8(9):e75245.
58. Aggarwal A, *et al.* (2017) Development of a Novel Lead that Targets *M. tuberculosis* Polyketide Synthase 13. *Cell* 170(2):249-259.e225.
59. Cox JAG, *et al.* (2016) THPP target assignment reveals EchA6 as an essential fatty acid shuttle in mycobacteria. *Nature Microbiology* 1(2):15006.
60. Willand N, *et al.* (2009) Synthetic EthR inhibitors boost antituberculous activity of ethionamide. *Nature Medicine* 15(5):537-544.
61. LeMagueres P, *et al.* (2005) The 1.9 Å Crystal Structure of Alanine Racemase from Mycobacterium tuberculosis Contains a Conserved Entryway into the Active Site. *Biochemistry* 44(5):1471-1481.
62. Munshi T, *et al.* (2013) Characterisation of ATP-Dependent Mur Ligases Involved in the Biogenesis of Cell Wall Peptidoglycan in Mycobacterium tuberculosis. *PLOS ONE* 8(3):e60143.
63. Chen C, *et al.* (2019) The Inhibitory Effect of GlmU Acetyltransferase Inhibitor TPSA on Mycobacterium tuberculosis May Be Affected Due to Its Methylation by Methyltransferase Rv0560c. *Frontiers in Cellular and Infection Microbiology* 9(251).
64. VanderVen BC, *et al.* (2015) Novel Inhibitors of Cholesterol Degradation in Mycobacterium tuberculosis Reveal How the Bacterium's Metabolism Is Constrained by the Intracellular Environment. *PLOS Pathogens* 11(2):e1004679.
65. Cohen-Gonsaud M, *et al.* (2002) Crystal Structure of MabA from Mycobacterium tuberculosis, a Reductase involved in Long-chain Fatty Acid Biosynthesis. *Journal of Molecular Biology* 320(2):249-261.
66. Gurcha SS, *et al.* (2014) Biochemical and structural characterization of mycobacterial aspartyl-tRNA synthetase AspS, a promising TB drug target. *PloS one* 9(11):e113568-e113568.
67. Wlodarchak N, *et al.* (2018) In Silico Screen and Structural Analysis Identifies Bacterial Kinase Inhibitors which Act with β -Lactams To Inhibit Mycobacterial Growth. *Molecular Pharmaceutics* 15(11):5410-5426.

68. Kang C-M, *et al.* (2005) The Mycobacterium tuberculosis serine/threonine kinases PknA and PknB: substrate identification and regulation of cell shape. *Genes & Development* 19(14):1692-1704.
69. Chiarelli LR, *et al.* (2018) A multitarget approach to drug discovery inhibiting Mycobacterium tuberculosis PyrG and PanK. *Scientific Reports* 8(1):3187.
70. Liu F, *et al.* (2017) Structure-Based Optimization of Pyridoxal 5'-Phosphate-Dependent Transaminase Enzyme (BioA) Inhibitors that Target Biotin Biosynthesis in Mycobacterium tuberculosis. *Journal of Medicinal Chemistry* 60(13):5507-5520.
71. Jansen RS, *et al.* (2020) Aspartate aminotransferase Rv3722c governs aspartate-dependent nitrogen metabolism in Mycobacterium tuberculosis. *Nature Communications* 11(1):1960.
72. Al-Shar'i NA, *et al.* (2019) Discovery of a nanomolar inhibitor of the human glyoxalase-I enzyme using structure-based poly-pharmacophore modelling and molecular docking. *Journal of Computer-Aided Molecular Design* 33(9):799-815.
73. Al-Shar'i NA, *et al.* (2021) Ellagic acid: A potent glyoxalase-I inhibitor with a unique scaffold. *Acta Pharmaceutica* 71(1):115-130.
74. Al-Shar'i NA (2020) Tackling COVID-19: identification of potential main protease inhibitors via structural analysis, virtual screening, molecular docking and MM-PBSA calculations. *Journal of Biomolecular Structure and Dynamics*:1-16.
75. Li J, Fu A, & Zhang L (2019) An Overview of Scoring Functions Used for Protein–Ligand Interactions in Molecular Docking. *Interdisciplinary Sciences: Computational Life Sciences* 11(2):320-328.
76. Krammer A, Kirchhoff PD, Jiang X, Venkatachalam CM, & Waldman M (2005) LigScore: a novel scoring function for predicting binding affinities. *Journal of Molecular Graphics and Modelling* 23(5):395-407.
77. Gehlhaar DK, *et al.* (1995) Molecular recognition of the inhibitor AG-1343 by HIV-1 protease: conformationally flexible docking by evolutionary programming. *Chemistry & Biology* 2(5):317-324.
78. Gehlhaar DK, Bouzida D, & Rejto PA (1999) Reduced Dimensionality in Ligand–Protein Structure Prediction: Covalent Inhibitors of Serine Proteases and Design of Site-Directed Combinatorial Libraries. *Rational Drug Design, ACS Symposium Series*, (American Chemical Society), Vol 719, pp 292-311.
79. Jain AN (1996) Scoring noncovalent protein-ligand interactions: A continuous differentiable function tuned to compute binding affinities. *Journal of Computer-Aided Molecular Design* 10(5):427-440.
80. Muegge I & Martin YC (1999) A General and Fast Scoring Function for Protein–Ligand Interactions: A Simplified Potential Approach. *Journal of Medicinal Chemistry* 42(5):791-804.
81. Muegge I (2006) PMF Scoring Revisited. *Journal of Medicinal Chemistry* 49(20):5895-5902.
82. Al-Balas QA, Hassan MA, Al-Shar'i NA, El-Elimat T, & Almaaytah AM (2018) Computational and experimental exploration of the structure–activity relationships of flavonoids as potent glyoxalase-I inhibitors. *Drug Development Research* 79(2):58-69.
83. Venugopala KN, *et al.* (2020) Anti-Tubercular Properties of 4-Amino-5-(4-Fluoro-3-Phenoxyphenyl)-4H-1,2,4-Triazole-3-Thiol and Its Schiff Bases: Computational Input and Molecular Dynamics. *Antibiotics* 9(9):559.
84. Schaeffer ML, *et al.* (2001) Purification and Biochemical Characterization of the Mycobacterium tuberculosis β -Ketoacyl-acyl Carrier Protein Synthases KasA and KasB. *Journal of Biological Chemistry* 276(50):47029-47037.
85. Bhatt A, Molle V, Besra GS, Jacobs Jr WR, & Kremer L (2007) The Mycobacterium tuberculosis FAS-II condensing enzymes: their role in mycolic acid biosynthesis, acid-fastness, pathogenesis and in future drug development. *Mol Microbiol* 64(6):1442-1454.

86. Schiebel J, *et al.* (2013) Structural Basis for the Recognition of Mycolic Acid Precursors by KasA, a Condensing Enzyme and Drug Target from *Mycobacterium tuberculosis*. *Journal of Biological Chemistry* 288(47):34190-34204.
87. Abrahams KA, *et al.* (2016) Identification of KasA as the cellular target of an anti-tubercular scaffold. *Nature Communications* 7(1):12581.
88. Luckner SR, Machutta CA, Tonge PJ, & Kisker C (2009) Crystal Structures of *Mycobacterium tuberculosis* KasA Show Mode of Action within Cell Wall Biosynthesis and its Inhibition by Thiolactomycin. *Structure* 17(7):1004-1013.
89. Dey S, Lane JM, Lee RE, Rubin EJ, & Sacchettini JC (2010) Structural Characterization of the *Mycobacterium tuberculosis* Biotin Biosynthesis Enzymes 7,8-Diaminopelargonic Acid Synthase and Dethiobiotin Synthetase. *Biochemistry* 49(31):6746-6760.
90. Singh S, Khare G, Bahal RK, Ghosh PC, & Tyagi AK (2018) Identification of *Mycobacterium tuberculosis* BioA inhibitors by using structure-based virtual screening. *Drug design, development and therapy* 12:1065-1079.
91. Dai R, *et al.* (2015) Fragment-based exploration of binding site flexibility in *Mycobacterium tuberculosis* BioA. *Journal of medicinal chemistry* 58(13):5208-5217.